THE MORPHOLOGY OF THE VERTEBROBASILAR SYSTEM

PhD thesis

László Szalontai MD

Doctoral School of Theoretical and Translational Medicine

Semmelweis University

Supervisor:	Ádám Domonkos Tárnoki MD, Ph.D
Official reviewers:	Dávid Sándor Győri MD, Ph.D
	Andrea Horváth MD, Ph.D

Head of the Complex Examination Committee: Dániel Bereczki MD, D.Sc

Members of the Complex Examination Committee: Edit Dósa MD, Ph.D
Ildikó Vastagh MD, Ph.D

Budapest
2021

TABLE OF CONTENTS

ABBREVIATIONS

AIC	Akaike information criterion
ARWMC	Age-related white matter changes
BA	Basilar artery
BIC	Bayesian information criterion
BMI	Body mass index
CI	Confidence interval
CT	Computed tomography
CTA	Computed tomography angiography
CVD	Cardiovascular disease
DICOM	Digital Imaging and Communications in Medicine
DZ	Dizygotic
FLAIR	Fluid attenuated inversion recovery
FSRP	Framingham Stroke Risk Profile
HU	Hounsfield unit
MIP	Maximum intensity projection
MR	Magnetic resonance
MRA	Magnetic resonance angiography
MRI	Magnetic resonance imaging
MV	Mean velocity
MZ	Monozygotic
OR	Odds ratio
PCA	Posterior cerebral artery
PI	Pulsatility index
SSD	Surface shaded display
SVU	Society for Vascular Ultrasound
TCCD	Transcranial color doppler
TCD	Transcranial color-coded duplex
TIA	Transient ischemic attack
TOF	Time-of-Flight
VA	Vertebral artery

VBI	Vertebrobasilar insufficiency
VMTK	Vascular Modeling Toolkit
VRT	Volume rendering technique
WMH	White matter hyperintensity
WSS	Wall shear stress

Symbols

l	Length	mm
r	Radius	mm
d	Diameter	mm
V	Volume	mm³
A	Area	mm²
κ	Curvature	%
τ	Tortuosity	%
∠	Angle	°
N	Torsion	%

1. INTRODUCTION

1.1. Anatomy of the vertebrobasilar system

The vertebrobasilar system consists of the two vertebral arteries (VAs) and the basilar artery (BA) and provides blood to the posterior part of the brain (**Figure 1.**).
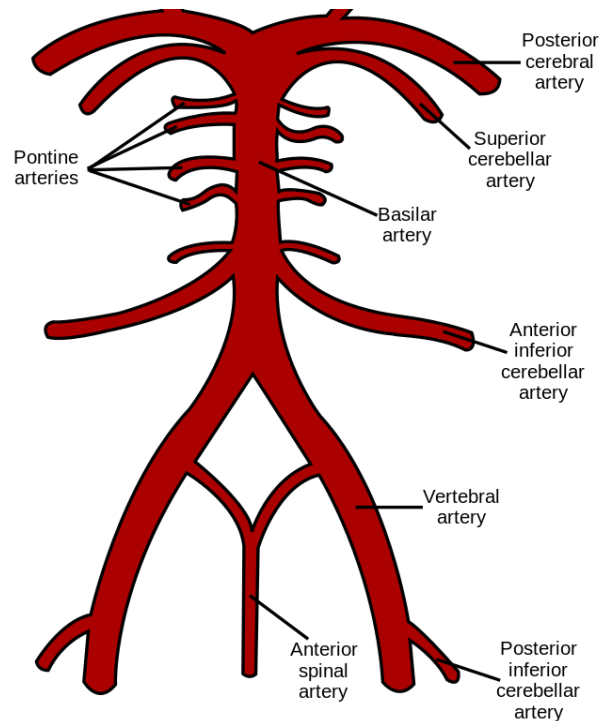
Figure 1.

Schematic representation of the vertebrobasilar system. Picture by Dimin **CC BY 3.0** (https://creativecommons.org/licenses/by/3.0/). Accessed: https://commons.wikimedia. org/wiki/File:Wils.png

In the most common anatomical variation, the two VAs originate from the left and the right subclavian artery. The V1 section of the VA is between the subclavian artery and the transverse foramen of the C6. The V2 section is between the transverse foramen of the C6 and the transverse foramen of the C2. The V3 section begins from the C2, then forms a loop around the arc of the atlas and continues to run upwards until it perforates the dura. The V4 section is between the dural perforation and the confluence where the VAs join to form the BA (**Figure 2.**).
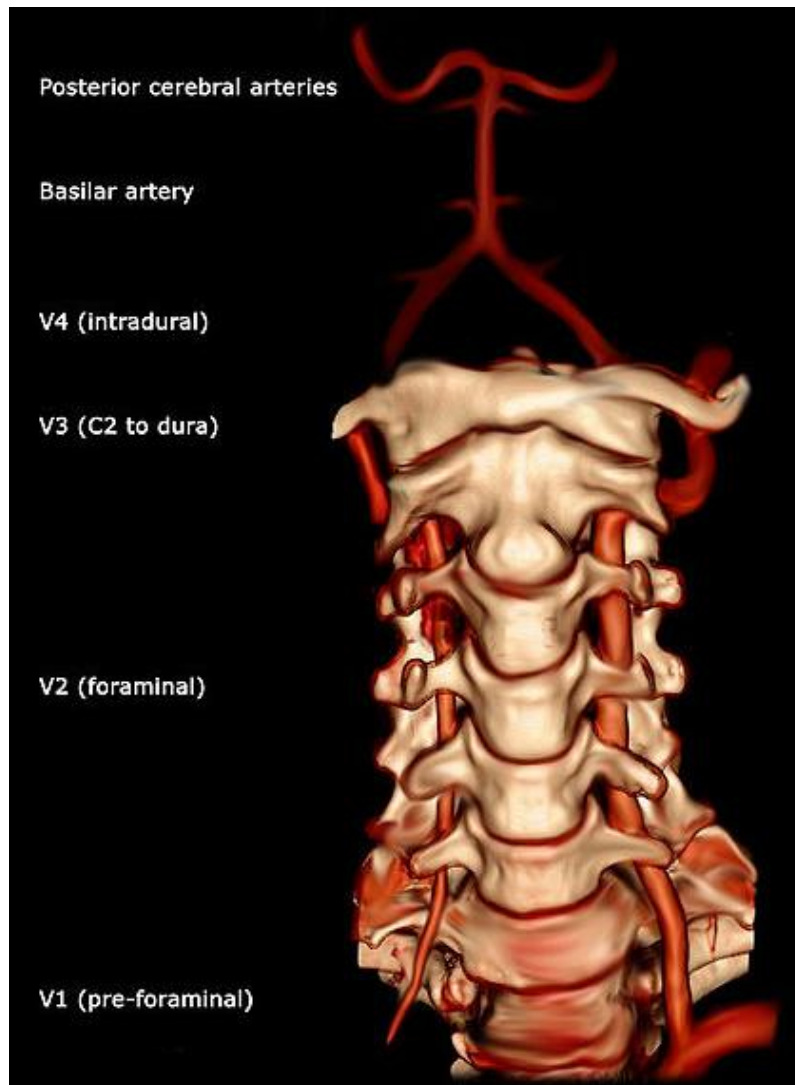
Figure 2.

Vertebral artery based on 3D surface rendered Computed tomography angiography. Picture by Frank Gaillard, distributed under a **CC BY-SA 3.0** license (https:// creativecommons.org/licenses/by-sa/3.0/deed). Accessed: https://es.wikipedia.org/wiki /Archivo:Vertebral_artery_3D_AP.jpg

The two main branches of the VA on each side are the anterior spinal artery, which supplies blood to the spinal cord and the myelencephalon, and the posterior inferior cerebellar artery, which supplies blood to the lower third of the cerebellum. The BA supplies the pons and the upper half of the tegmentum with short paramedian arteries, as well as circumferential branches to the base of the pons and the outer two-thirds of the tegmentum. The two posterior cerebral artery (PCA) originate from the

BA, and their branches can be grouped according to their supplied area. These branches supply the brain stem, the midbrain, and the lateral and medial areas of the: occipital, temporal, and parietal lobes of the cortex. The anterior inferior and superior cerebellar arteries also originate from the BA, which supplies blood to the pons, the upper two third of the cerebellum, the inner ear, and the roots of the vagal and glossopharyngeal nerve [1-3]. The vertebrobasilar system joins the circle of Willis posteriorly via the two PCA and the two posterior communicating arteries (**Figure 3.**). The vertebrobasilar system is unique in anatomical terms, as it is the only instance in the human body where a third artery is formed by the merging of two arteries.
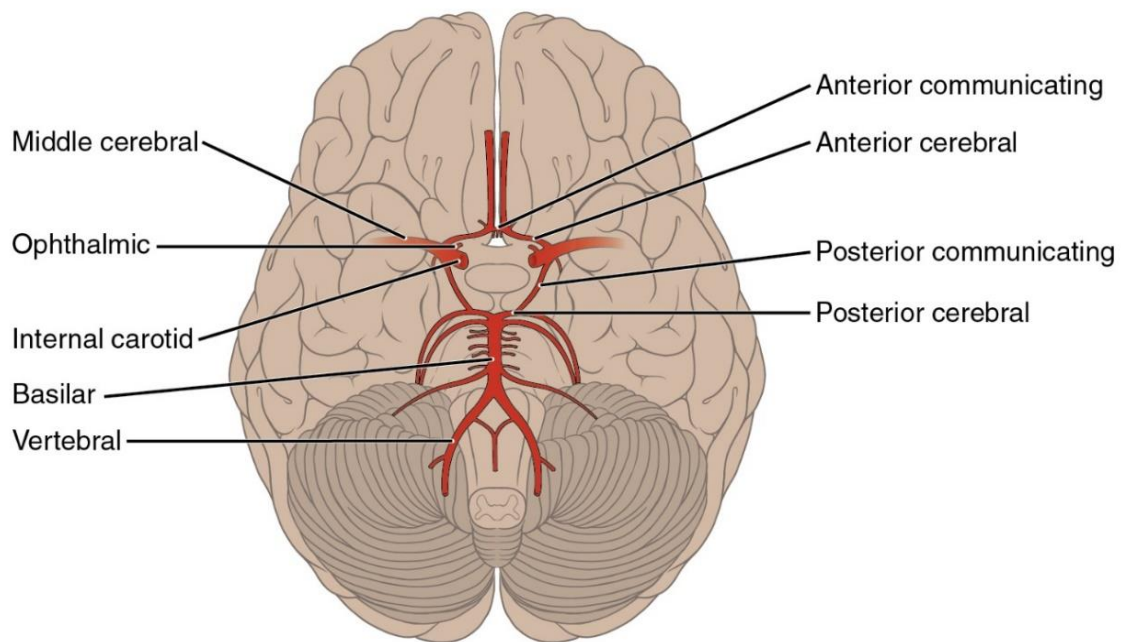
Figure 3.

The Circle of Willis and the vertebrobasilar system. Illustration from Anatomy & Physiology, Connexions Web site, distributed under **CC BY 3.0** license (https:// creativecommons.org/licenses/by/3.0/). Accessed: https://commons.wikimedia.org/wiki /File:2123_Arteries_of_the_Brain.jpg

1.2. The anatomical layers of the studied arteries

There are 3 types of arteries: Elastic, muscular and resistance arteries consisting of smaller arteries and arterioles (**Figure 4.**). Most arteries are comprised of three layers: the tunica intima, media, and externa.
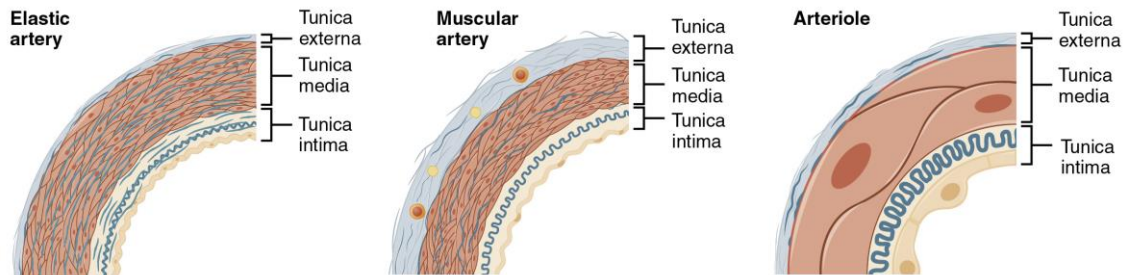
Figure 4.

The anatomical layers of the arteries. Illustration by OpenStax College Anatomy & Physiology, distributed under **CC BY 3.0** license (https://creativecommons.org/licenses /by/3.0/). Accessed: https://commons.wikimedia.org/wiki/File:2103_Muscular_ and_Elastic_Artery_Arteriole.jpg.

The VAs can either be considered as elastic or muscular arteries based on the composition of the vessel wall. The wall composition slowly transitions along the entire length of the VA. From the origin up until 1 cm proximal to the dural perforation they are considered as elastic arteries due to their thick tunica adventitia and external elastic lamina [4]. Otherwise known as Windkessel arteries, these arteries contain larger numbers of collagen and elastin filaments in their tunica media compared to muscular arteries. This gives them the ability to stretch in response to each heart pulse. The larger number of elastic fibers give increased elasticity to these arteries which allow the Windkessel effect to maintain relatively constant pressure in the arteries despite the pulsating nature of the blood flow from the heart [5].

The intracranial V4 segments of the two VAs and the BA are considered as muscular arteries [4, 6]. Otherwise called distributing arteries, these mid-sized vessels draw blood from the elastic arteries and branch into the smaller resistance vessels, including small arteries and arterioles. In contrast to the elastic arteries which store and dissipate the energy generated by the systolic contraction, muscular arteries contain

fewer elastic components and a higher number of layers of smooth muscle providing involuntary control of vessel caliber and thus control of blood flow. Muscular arteries are identified by the well-defined elastic lamina that lies between the tunica intima and media [5].

1.3. The morphological indices of blood vessels

Morphology is the study of form or structure of an organism or any of its parts [7]. To accurately measure the morphological indices of the vertebrobasilar system we first need to define these measurable variables. In simplified terms all blood vessels can be considered as non-perfect tubes. These structures have an imaginary centerline along their entire length which can be defined as the weighted shortest paths traced from the middle of the vessel wall [8]. The length (l) of any vessel can be defined as the length of their centerline (**Figure 5.**).
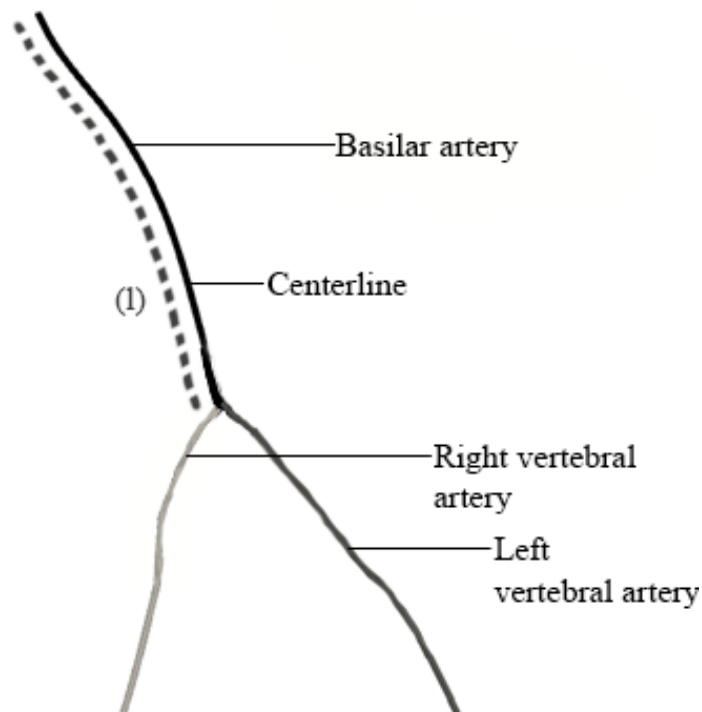
Figure 5.

Visual representation of the centerlines in the vertebrobasilar system and how the length (l) of different arteries is measured. Own picture.

Because blood vessels are non-perfect tubes their radius (r) and diameter (d) constantly change at different points along their centerline. The radius of a vessel is the distance from the centerline to the vessel wall. The diameter (d) of a vessel is the distance from one point of the vessel wall through the centerline to another point of the wall (d = 2 × r). Because vessel radius and diameter is a dynamic variable along the centerline multiple measurements are needed on different points along the centerline [9]. The greater the number of these measurement locations the better we can estimate a vessels average radius and diameter (**Figure 6.**). The volume (V) of a tubelike structure can be obtained by multiplying its base area ($A = r^2 \times \pi$) by its length (l) V = A × l. To measure the volume of arteries we need to use different software's built in measurement tools (such as VMTK) [9] **(Figure 6.)**. Average area of an artery can be obtained by dividing the volume of an artery by its length. However, this may cause false correlations during the statistical analysis due to the calculation method.
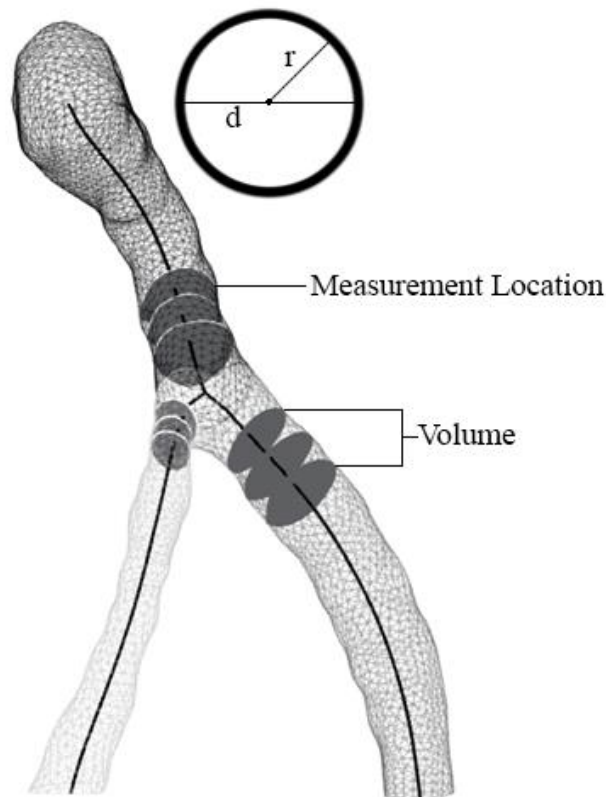
Figure 6.

Visual representation of how radius (r), diameter (d) and volume (V) are measured. Own picture.

The geometry of a three-dimensional vascular centerline can be described with the help of the Frenet-Serret system. This approach uses 3 perpendicular vectors (tangent, normal and bi-normal) originating from a point on the centerline. Using these vectors different spatial geometrical indices such as curvature (κ) and torsion (N) can be derived. Curvature is the amount by which a curve deviates from being a straight line. The curvature at the measurement location is the reciprocal of the radius of the osculating circle, in units of radians per unit distance [9]. Tortuosity (τ) describes how many turns a vessel has and the simplest way to calculate it is to divide the length of the curve by the shortest distance between its end points [9] (**Figure 7.**). If we analyze multiple connecting vessel's relationship to each other, we can measure the angle ($\angle$) between the connecting centerline's vectors [9]. Torsion of a vessel can be defined by the extent it is rotating out of the pre-defined plane of reference around its vectors [9, 10] (**Figure 7.**). Finally, we can measure the extent and the laterality of a vessels bending (curving) if we connect the two end points of the vessel with a straight line and measure the deviation from this line on a fixed plane.
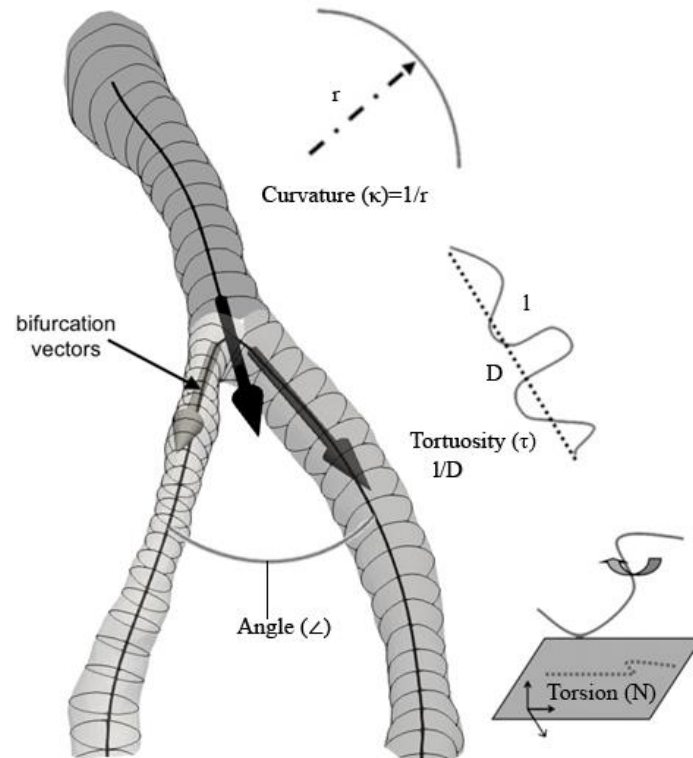
Figure 7.

Visual representation of how curvature (κ), tortuosity (τ), torsion (N) and bifurcation angle ($\angle$) are measured. Own picture.

1.4. Geometrical variations of the vertebrobasilar system

The confluence of the vertebrobasilar system has been qualitatively classified into four main categories: Tuning fork, Walking, Lambda and No confluence [11] (**Figure 8.**).
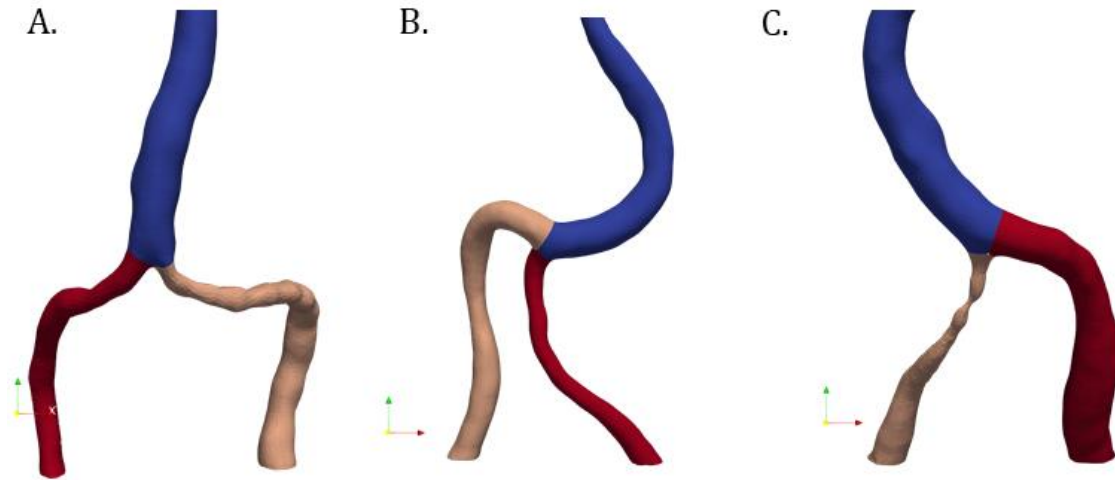
Figure 8.

The main types of geometrical variations of the vertebrobasilar system. The left (tan) and right V4 section of the vertebral artery (red) can be seen with the basilar artery (blue). **A.** Tuning fork geometry. **B.** Walking geometry. **C.** Lambda – Dominant subtype. Own picture.

The tuning fork geometry consist of two approximately equal diameter VAs (difference less than 0.3 mm) which bend in opposite directions towards the vertebrobasilar confluence (**Figure 8. / A.**). The two VA join in a rather symmetrical angle to from the BA. In this geometry the BA continues in a relatively straight line to the BA top without bending. The walking geometry consist of two equal diameter VAs (difference less than 0.3 mm) which bend in the same direction towards the vertebrobasilar confluence (**Figure 8. / B.**). The two VAs join in a narrow angle to form the BA. VA angle can vary between 10° to 160° and symmetrical VA mean is approximately 70° [12]. In this geometry the basilar artery shows an opposite bending direction compared to the two VAs and has an increased curvature along its centerline to the basilar top. The lambda geometry has two subtypes: Dominant-lambda and Hypoplastic-lambda. The dominant-lambda subtype consists of unequal VA diameters

where the BA continues along the centerline of the dominant VA. In the majority of the cases this leads to an opposite direction bending and increased curvature of the BA (**Figure 8. / C.**). Hypoplastic-lambda is the less common subtype compared to its dominant counterpart [11]. This geometry also consists of unequal VA diameters; however, the BA continues along the centerline of the non-dominant VA, and it may lead to a same direction bend and increased curvature of the BA. In the "no confluence" geometry, the non-dominant VA does not join the vertebrobasilar confluence and usually ends as the posterior inferior cerebellar artery. The dominant VA extends along its centerline to become the BA. The geometry of the vertebrobasilar junction has a large influence on the flow in the basilar artery. Different vertebrobasilar geometries may cause complex flow patterns and low inconsistent wall shear stress. This is associated with atherosclerosis, increased curvature and tortuosity over time [13].

1.5. Morphological changes induced by wall shear stress

Shear stress is defined as the frictional force generated by blood flow in the endothelium, that is, the force that the blood flow exerts on the vessel wall, expressed in force-area unit (N/m^2 or Pa) [14]. A great generalization is that high laminar shear stress is atheroprotective, while low shear stress and/or oscillating shear stress tends to enhance atherogenicity [15]. The average wall shear stress (WSS) in the vertebrobasilar confluence ranges between 4.5 to 9.2 Pa in healthy individuals [10] (**Figure 9.**).
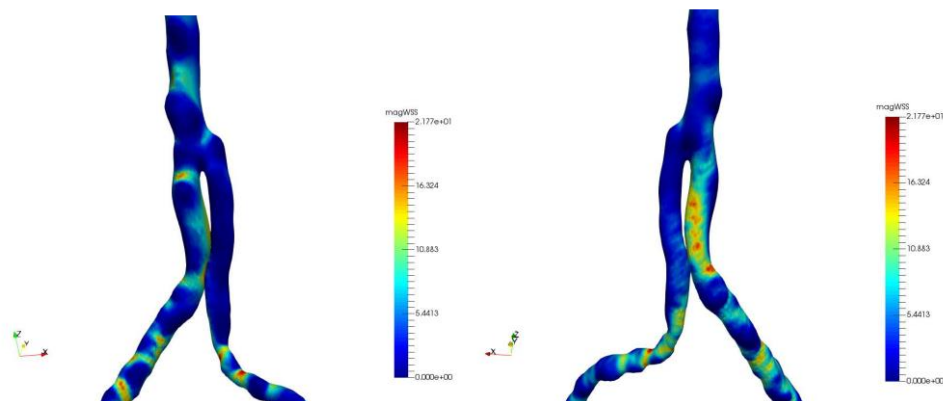
Figure 9.

Wall shear stress magnitude distribution in a healthy individual, posterior (left) and anterior (right) view. Image courtesy of Dániel György Kalácska.

13

The endothelium is the primary sensor for WSS. Changes in shear stress may lead to instantaneous vasomotor changes which are regulated on a beat-to-beat basis in order to maintain constant shear stress and optimize artery blood flow and distribution. Continuous oscillation in WSS are associated with higher rates of lipoprotein oxidation [16], increased endothelial apoptosis [17], and higher risk to develop atherosclerotic plaques (**Figure 10.**).
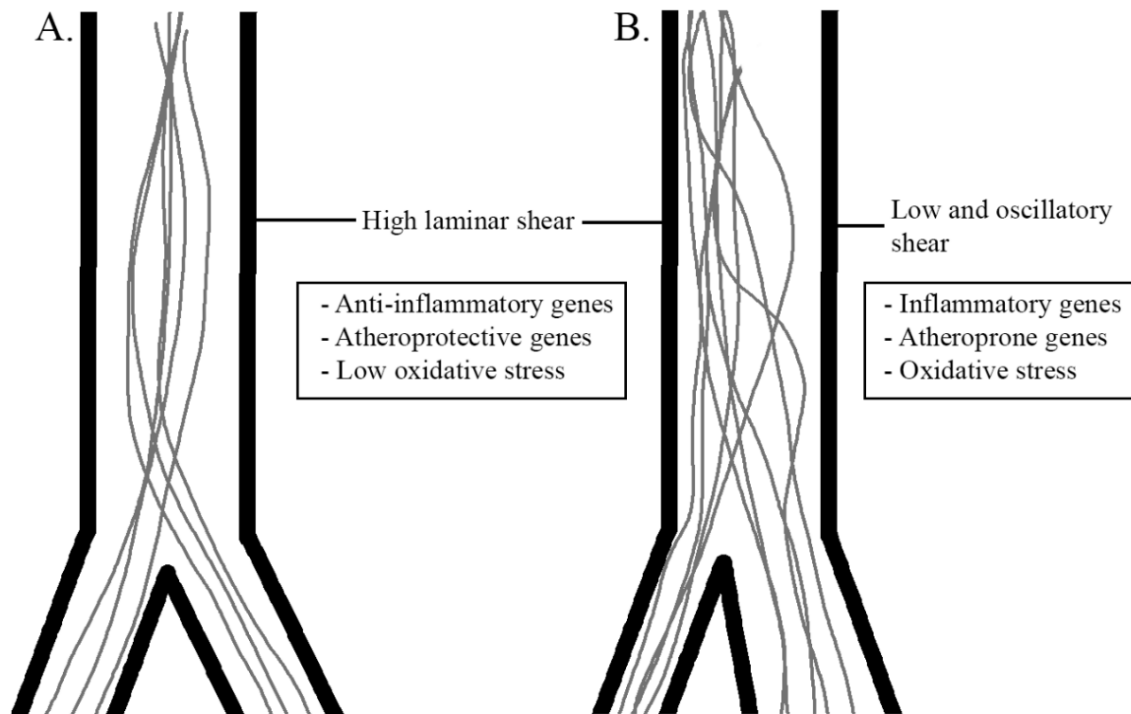
Figure 10.

Symmetrical (**A.**) and asymmetrical (**B.**) vertebrobasilar junction. On picture **A.** continuous high laminar shear can be observed which is atheroprotective. On picture **B.** one side of the basilar artery has relatively undisturbed high laminar shear while the opposite side has low and oscillatory shear which is atheroprone. Own picture.

Unequal hemodynamic forces in an artery will alter cellular responses, facilitating equilibration to return the blood flow and shear stress to a more constant level. Past animal studies addressed how repeated exposure to high blood flow and decreased WSS over prolonged time affect arterial remodeling [18, 19]. In unequal flows of joining arteries one side of the newly formed artery has low and oscillating WSS, which stimulates intimal thickening. The other side has high blood flow which

leads to lumen enlargement and elongation of the artery along with increased tortuosity [19-21].

The same principals can be applied to human physiology. Amongst the cerebral vessels increased tortuosity often occurs in the BA, the communicating, anterior and PCAs and in the arterioles in the brain white matter [22-24]. In the BA, high blood flow and increased WSS lead to arterial enlargement, elongation, and increased tortuosity. This includes smooth muscle cell and endothelial cell proliferation, and migration [25]. Low WSS leads to arterial shortening and constriction, with intima-media proliferation and thickening. This reduces lumen diameter and thus tends to normalize WSS levels. These two adaptive changes over prolonged time periods result in arterial bending and increased tortuosity. Increased arterial tortuosity of cerebral arteries has been associated with elder, hypertensive patients [22, 23] and with patients with Moyamoya-disease [26]. Cerebral arteries may also become tortuous due to malformation or increased flow associated with elastin degradation [24].

1.6. Atherosclerosis and Vertebrobasilar Insufficiency

1.6.1. Atherosclerosis of the basilar artery

Atherosclerotic plaques often arise in locations with complex flow patterns [12, 27]. The pathomechanism consist of accumulation of fats, cholesterol and/or fibrous material in the intima of the arterial wall, the innermost layer of the vessels. The localization, size, structure (homogeneous, inhomogeneous, calcareous) and surface features (smooth, uneven, ulcerated) of plaques should be determined, as they all have prognostic significance. The current most acceptable theory is that low WSS is one of the key driving factors in atherosclerotic plaque development and location [28]. Vertebrobasilar geometry strongly influence BA plaque location [28, 29]. The highest prevalence for plaques can be observed in the walking geometry, while the lowest in the Tuning fork geometry [11]. The majority of plaques can be on either the left or right side of the BA (blocking perforating side branches) or on the dorsal wall depending on the vertebrobasilar confluation geometry proximal to the junction [29, 30]. Zhou et. al

found significantly more plaques on the small curve of tortuous BAs and higher BA tortuosity in patients with BA plaques [27]. Deng et. al found that BA tortuosity and bending was independently associated with the presence, severity, and location (mainly on the small curve of the BA) of atherosclerotic plaques [31]. Risk factors for atherosclerosis include hypertension, smoking, diabetes, hyperlipidemia and increased body mass index (BMI) [32].

1.6.2. Vertebrobasilar Insufficiency

Vertebrobasilar Insufficiency (VBI) can be defined as inadequate blood perfusion of the posterior circulation. VBI can describe short term and recurring symptoms but also severe acute events such as transient ischemic attack (TIA) or posterior stroke. The main symptoms of VBI are vertigo, dizziness, diplopia, paresthesia, confusion, dysphagia, headache or ataxia [33]. VBI can be caused by two processes: hemodynamic disturbance caused by either narrowing of the vessels or embolism. The most common cause for arterial stenosis (narrowing) is due to atherosclerosis, however it can be also caused by arterial dissection, fibromuscular dysplasia, migraine, trauma or external compression [33]. Usually, symptoms due to stenosis of a single artery tend to be short term and reproducible, rarely causing ischemia. For ischemia and stroke to occur occlusion must be present in both VAs or in the BA. In addition, inadequate blood flow contribution must be present due to one or both posterior communicating artery being hypoplastic or occluded [33, 34]. Subclavian steal syndrome causes VBI due to reversed VA flow stealing blood flow from the brainstem. VBI caused by emboli can be categorized based on where they originate from. Two-third of the emboli form extracranially and originate from atherosclerotic lesions located in the subclavian or vertebral arteries [35]. Up to one-third of the lesions originate intracranially [36]. While a small portion of these emboli are formed by basilar artery aneurysms which may then embolize to more distal branches [36].

1.7 Age-related white matter hyperintensities on Fluid Attenuated Inversion Recovery (FLAIR) MRI sequence

Age-related white matter hyperintensities (WMH) are common FLAIR MRI findings of asymptomatic patients, and their prevalence grows with age. FLAIR is a special sequence where to null the signal of the cerebrospinal fluid on a T2 weighted image we adjust the inversion time as such that at equilibrium there is no net transverse magnetization of the cerebrospinal fluid. With this sequence grey matter is brighter than white matter, while the cerebrospinal fluid is void of signal. This sequence is very sensitive to pathological changes (they appear as bright areas) and makes the differentiation between cerebrospinal fluid and an abnormality much easier [37]. Approximately 20-55% of 60-year-old (depending on study) and almost 100% of 90-year-old patients have Age-related WMHs [38]. WMH burden is higher in patients with hypertension, diabetes, hyperlipidemia, a history of cognitive impairment, dementia or vascular disorders [39]. WMHs can be distinguished into two groups: periventricular and deep WMH. Periventricular WMH, which is associated with a combination of demyelination, ependymitis, and granular and subependymal gliosis. Deep WMH is associated with small subcortical infarcts or with a process called incomplete infarction, reflecting chronically reduced blood flow in deep areas of the brain caused by arteriolosclerosis [40].

Deep WMH increases the risk of stroke by 3 folds [41, 42]. The exact method for separating Deep WMHs from Periventricular WMHs is still under debate. Currently it can be achieved by the combination of continuity to the ventricles [43, 44] or if no continuity can be seen, a 10 mm distance from the ventricles rule can be applied [44]. Deep WMH severity can be classified based on the age-related white matter changes (ARWMC) score: 0 = no confluence 1 = focal lesions; 2 = beginning confluence; 3 = diffuse involvement of the entire region [45] (**Figure 11.**).
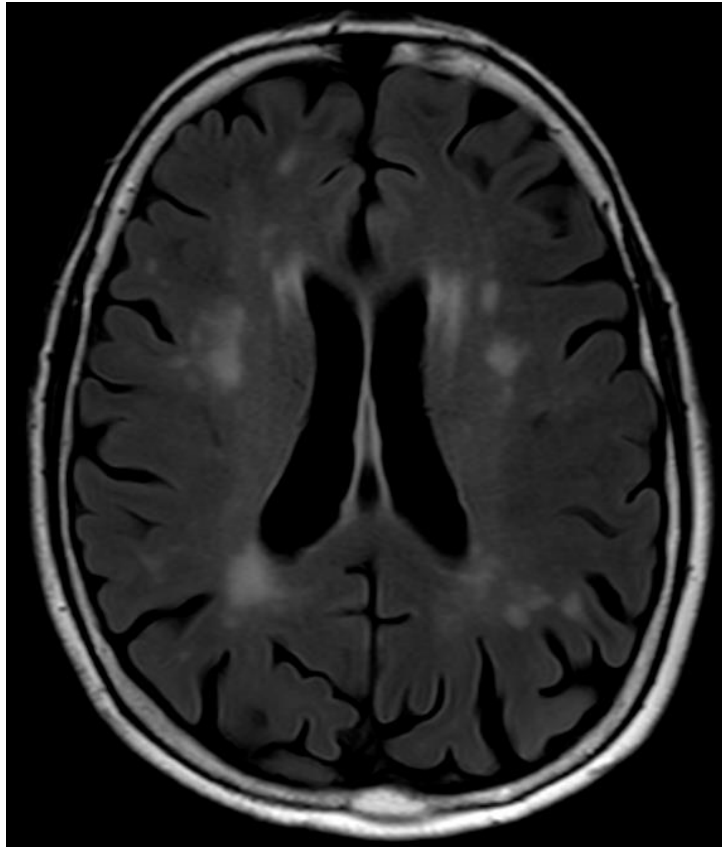
Figure 11.

Age-related white matter changes (ARWMC) score 2 on T2 FLAIR MRI sequence (Source: Medical Imaging Centre, Semmelweis University, Budapest, Hungary). Own picture.

1.8. Vascular imaging of the vertebrobasilar system

1.8.1. Transcranial Doppler

Transcranial Doppler (TCD) is a non-invasive, safe, and cost-effective. It does not involve radiation exposure and can be performed at the bedside of the patient to evaluate the cerebrovascular circulation. With TCD, we can capture real-time hemodynamic information about brain circulation, as opposed to static images with other techniques (**Figure 12.**). TCD is considered effective in the detection of stenosis, occlusion and vasospasm in the vertebrobasilar system using transforaminal insolation [46].
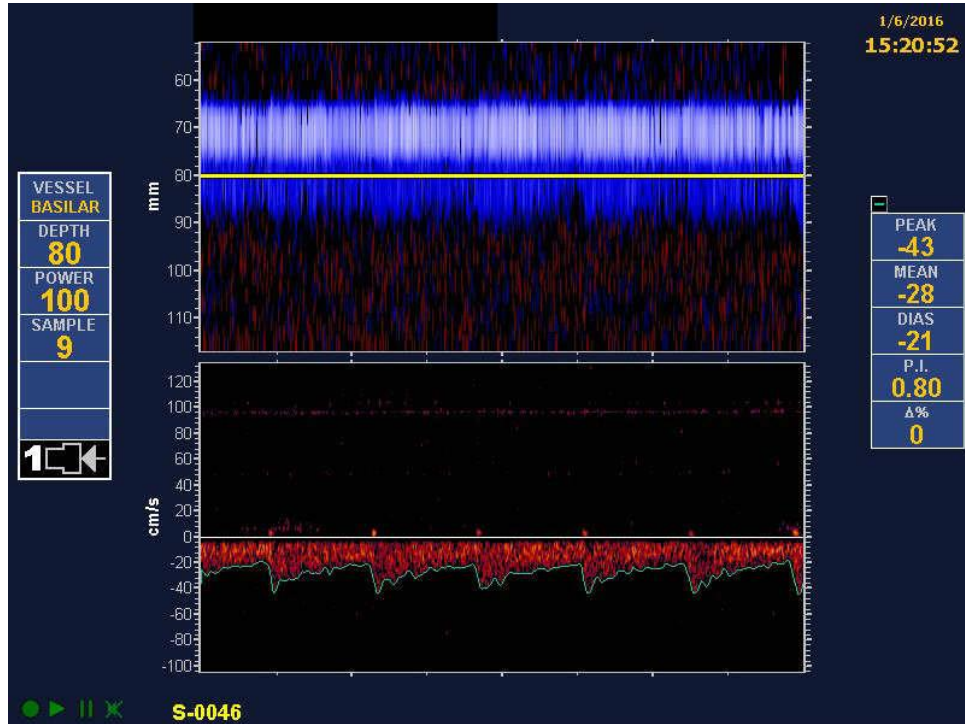
Figure 12.

Transcranial Doppler of the basilar artery from the suboccipital window. Image courtesy of Zsolt Garami, MD.

A TCD machine consists of a monitor and a 2-2.5MHz pulse doppler. The hardware has to be capable of pulse wave analysis and real-time display of the following data: measured flow depth, mean velocity (MV), pulsatility index (PI), transducer power and frequency, maximum flow rate, end-diastolic speed and automatic emboli detection [47]. The probe uses insonation windows, which are bone regions with thinner bone-wall along the side of the skull that allows measurements. Once the artery in question is found, blood flow velocities are measured with the pulsed Doppler effect probe, which creates a graph with blood flow velocities over time [48]. Together, these make a duplex test. Indications for TCD testing include according to the Society for Vascular Ultrasound (SVU) [47]: intracranial stenosis or occlusion, vasospasm following subarachnoid hemorrhage, follow-ups of arteriovenous malformations, diagnosis of vertebrobasilar circulatory disorders, intracranial flow measurements following head injuries, different measurements in sickle cell anemia, vasomotor reactivity tests after administration of certain drugs and intracranial flow monitoring

19

during cardiovascular surgery [49]. The method can also be used to detect and measure blood flow in the middle cerebral artery part M1 and M2, the intracranial segments of the internal carotid artery, the anterior cerebral artery, the PCA part P1 and P2 and the posterior communicating arteries of the circle of Willis [47]. There are no contrast agents used with the TCD technique.

1.8.2. Transcranial Color Doppler

Transcranial Color Doppler (TCCD) is a method that can be used for monitoring intracranial blood-flow. Similarly, to TCD, TCCD uses the same special insonation windows (temporal, suboccipital, and ophthalmic) to gain insight into the intracranial space. TCCD uses an ultrasound machine equipped with a sector transducer with an operating frequency of 2.0–3.5 MHz with a small aperture size to visualize intracranial vessels. It is ideal to set TCCD to B mode since this mode allows 2D imaging of the brain and skull structures [50]. Next, the color Doppler mode is activated to render the basal cerebral arteries visible (**Figure 13.**).
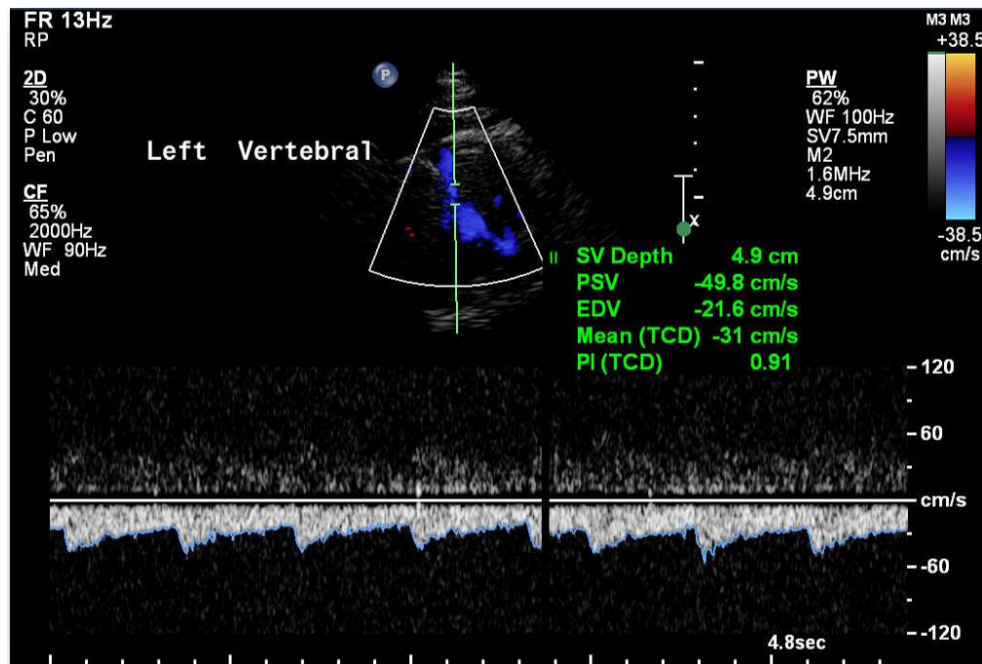
Figure 13.

Transcranial Color Doppler of the Left Vertebral artery. Image courtesy of Zsolt Garami, MD.

TCCD can visualize and measure blood flow of the proximal 2/3 of the BA and the V3/4 section of the vertebral artery from the suboccipital window and both PCAs from a temporal window [50, 51]. Yang et. al. showed that TCCD can reliably detect BA stenosis and refined a diagnostic criteria to detect <50%, 50-70% and >70% stenosis [52]. There are no contrast agents used with the TCCD technique.

1.8.3. Computed Tomography Angiography

Computed Tomography (CT) should be the first examination in acute head trauma cases, suspected acute cerebral vascular events, examination of fine bone structures, and the method can separate cerebral ischemic and hemorrhagic stroke accurately. It is also used as an alternative when MRI is contraindicated or not available. During every scan, the patient is exposed to ionizing radiation, which above a certain threshold has harmful effects on the human body and as such should be used only with appropriate indication [53].

Maximum intensity projection (MIP) allows the radiologist to select data in any Hounsfield unit (HU) attenuation range and leave out the rest. MIP allows the vessel walls and plaques within them to be better visualized (**Figure 14.**). 3D shaded surface display (SSD) is a CT technique that recognizes tissue by its density and creates a three-dimensional view of the vasculature within the acquired volume set. 3D volume rendering (VRT) is a newer, less operator involved technique that takes the entire volume of data and calculates each voxel along a line from the viewer's eye [54] (**Figure 14.**). CT-angiography (CTA) requires intravenous contrast administration. The rapid administration of a high iodine (350-400 mg I/ml) contrast agent (4 ml / sec) can create an ideal intravascular enhancement of the vertebrobasilar system [55]. CTA can detect VA stenosis from 70% reliably [56]. On non-contrast CT BA occlusion may appear hyperdense in 65% of the cases, similarly as the hyperdense MCA sign [57, 58]. BA occlusion on contrast enhanced CTA presents as filling defect in the vessel [57]. Shon et. al tested the clinical application of cerebral artery calcification on brain CT. They found that cerebral arterial calcification did not directly indicate hemodynamically significant stenosis of an artery segment, but may indicate a diffuse and severe

atherosclerotic process being present in the cerebral circulation [59].

Figure 14.

CT angiography sagittal MIP reconstruction (left) and volume rendered CT angiography (right) of the same patient. (Source: Medical Imaging Centre, Semmelweis University, Budapest, Hungary). Own picture.

1.8.4. Magnetic Resonance Angiography

Magnetic Resonance Angiography (MRA) is one of the most pursued modality for vertebrobasilar imaging often only limited by local capabilities [60]. MRI, compared with CT, has superior soft-tissue characterization, and lacks ionizing radiation. High-resolution-MRI has the capability to differentiate between plaque components and analyze the water content, chemical composition, molecular motion, and physical state. These parameters can help to characterize fibrocellular, lipid-rich, and calcified regions of atherosclerotic arterial plaques [61]. T1-weighted and time-of-flight sequences can be used to visualize intraplaque hemorrhage, while T2 and proton density sequences can differentiate between the plaque cap and the lipid core [62].

In conventional sequences, the flowing blood is signal-free, because when the pulse of the radio frequency is transmitted, the excited protons are replaced by non-excited protons in that slice. The advantages of contrast enhanced MRA is relative to other MRA techniques and include shorter acquisition times, improved anatomical coverage, and decreased susceptibility to artifacts caused by blood flow and pulsatility.

22

MRI contrast agents can be divided into 3 groups: paramagnetic, superparamagnetic and ferromagnetic contrasts [63]. The most common paramagnetic contrast agent used is gadolinium 3^+ based. Gadolinium creates a strong T1 signal and accumulates extracellularly because it cannot diffuse through the blood-brain barrier [64]. Iron is a superparamagnetic contrast media, which accumulates intracellularly and induces an inhomogeneous magnetic field to shorten T2 relaxation, producing a strong T2 signal [63]. Ferromagnetic contrast agents do not contain protons and only act on local hydrogen nuclei [63]. Even without contrast, MRI can detect blood flow and vessel wall in multiple planes.

Non-contrast MRA has been used for intracranial imaging. Its widespread use has been limited by prolonged acquisition times and motion artifacts. However, improvements in MRI hardware and software and concerns over the safety of gadolinium contrast agents in high-risk patients contributed to renewed interest. Time-Of-Flight (TOF) is the most used non-contrast MRA technique, especially for peripheral and intracranial vessels [65] (**Figure 15**).

Figure 15.

Maximum intensity projection (MIP) of a Time-Of-Flight (TOF) magnetic resonance angiography (MRA) of the circle of Willis, coronal view. (Source: Medical Imaging Centre, Semmelweis University, Budapest, Hungary). Own picture.

This sequence type is a gradient echo sequence with short repetition echo time, acquired with slices perpendicular to the direction of blood flow. Flowing blood moves unsaturated spins from outside the slice into the imaging plane. These completely relaxed spins produce a much higher signal and create a bright vascular image without contrast agent [65]. This flow-related enhancement is also referred to as a slice entry phenomenon. Because the phenomenon is flow related, we only see the blood flow and not the anatomical walls of the vessels. TOF acquisitions can be performed using 2D or 3D sampling, with 3D TOF being most often used for intracranial vasculature due to the tortuous nature of the arterial tree which needs higher spatial resolution [64]. The other two major non-contrast MRA techniques currently used are Phase-Contrast MRA and Steady-State Free Precession MRA [64].

1.9. Summarizing data from the literature

Morphological changes of the vertebrobasilar system require decades to form [66]. Asymmetrical complex blood flow patterns may lead to unequal and oscillating WSS which drives the morphological changes [10, 12, 25]. These changes are highly age related and tend to increase with hypertension and diabetes mellitus [67, 68].

VAs, in the majority of time, are congenitally asymmetrical and mainly left dominant. One side dominance of VA causes basilar bending to the opposite side [66, 67, 69]. This phenomenon increases as the vertebral difference increases [66, 67, 69, 70]. Increased VA diameter difference, tortuosity, and torsion alongside with increased BA curvature and tortuosity further causes inconsistent and complex blood flow patterns, which plays an important role in the pathogenesis of atherosclerosis [13, 27, 29, 71]. Furthermore, it has been shown that the posterior circulation is much more susceptible to atherosclerosis in comparison with the anterior circulation [72]. These vertebrobasilar morphological indices have also been linked to peri-vertebrobasilar infarcts as risk factors and have indicated directional and locational correlation [66, 69, 73]. Studies on these changes were predominantly conducted on the Asian populations. Amongst the Asian population one of the most common causes of stroke is intracranial stenosis or occlusion. In contrast, in the Caucasian population this is unlikely, and

stroke is mainly caused by the embolization of thrombi formed in the heart and along cervical vessels [74].

Although changes of the vertebrobasilar morphological indices has been associated with stroke and atherosclerotic plaque localization, the understanding of the genetic and environmental determinants influencing the development of these indices are not yet clear. This is where twin studies can help. Our research group in 2017 demonstrated heritability of the extracranial section of the VAs and VA diameter difference [75]. However, research focusing on the heritability of the different morphological indices of the intracranial vertebrobasilar system are scarce and needs further attention.

Increased WHM burden has been considered as an indicator for inadequate blood perfusion [76-78]. Multiple studies suggest that ischemia plays the most cardinal role with tortuous arterioles and reduced cerebral blood flow alongside histological changes, however, despite the past 2 decades of advancements in regarding the etiology of these processes there is still much uncertainty [79]. Recent studies suggest that the WMH burden can be related to TIA severity [80], first and second stroke risk [81] and post-stroke rehabilitation [82]. Furthermore, a strong relationship has been shown between the Framingham Stroke Risk Profile (FSRP) including its component risk factors and WMHs providing even more evidence for a vascular basis [83].

WMHs are suspected to be multifactorial in origin and as such are affected by genetic and non-genetic factors. In twin studies higher heritability was found for WMH in women [84, 85] and after adjusting for brain volume, women had more WMH than men. A recent study in 2018 showed significant moderate-to-high monozygotic twin correlations in WMHs in all brain regions (highest in the frontal lobe and lowest in the occipital lobe) [84]. This implied that vascular risk factors affect anatomical lobes differently. Deep WMH has shown higher heritability compared to periventricular WMH which suggests that periventricular WMH has higher environmental factor influence [85].

25

1.10. The importance of twin studies

Twin studies aim to resolve the debate of nature versus nurture. These studies attempt to distinguish between the traits received due to genes at birth and phenotypes that emerge by the different environmental factors during our lifetime [86]. These studies provide a strong basis for understanding the importance of any potential risk factors on a trait by controlling the genetic variations. It is known that monozygotic (MZ) twins share nearly 100% of their genome, while dizygotic (DZ) twins share roughly 50% of their genome in respect to a given phenotype [86]. We use this knowledge in the classical twin study. For example, higher levels of the intra-pair correlation between MZ pairs compared to DZ twins indicate a greater genetic influence on a phenotype, while a greater cross MZ and DZ twin similarity suggests that the variance is due to shared environmental factors. Using ACE univariate genetic modeling we can decompose these correlations into percentages showing us how heritability, or additive genetic factors (A), shared (C), and unique (E) environmental effects are affected by the trait we investigate [87].

2. OBJECTIVES

Our aim was:

- to investigate the intracranial vertebrobasilar morphology in a Caucasian population non-invasively with individually reconstructed 3D vessel models,
- to measure the morphological indices automatically on our models,
- to investigate the influence of the VA dominance on BA geometric indices,
- to investigate whether the BA geometry contributed to the existence and laterality of WMHs,
- to measure the heritability of each measured morphological vessel index using a classical twin study model.

Our hypothesis was:

- that most of the vertebrobasilar morphological changes demonstrated in the Asian population can also be found in a Caucasian population,
- that these changes are influenced by genetic factors,
- that the vertebrobasilar system morphology can influence the location of WMHs found on MRI FLAIR sequences.

In order to investigate these research hypotheses, two studies have been performed on two different patient groups:

1) a retrospective analysis of patients who underwent brain MRI (Study 1. "Laterality of deep white matter hyperintensity correlates with basilar artery bending and vertebral artery dominance"),
2) a prospective healthy twin study (Study 2. "Are the Morphological Indices of the Vertebrobasilar System Heritable? A Twin Study Based on 3D Reconstructed Models").

3. METHODS

3.1. Study 1. Laterality of deep white matter hyperintensity correlates with basilar artery bending and vertebral artery dominance

3.1.1. Patients

In this research, we retrospectively selected patients who visited the Medical Imaging Centre, Semmelweis University between 2017 and 2018, and underwent non-contrast brain MRI. Most patients were referred from the Department of Neurology for the following reasons: visual impairment, headache, or dizziness. Comorbidities such as hypertension, hyperlipidemia, and diabetes were gathered from the medical chart reports. The exclusion consisted of a medical history of large vessel obstruction, stroke, vasculitis, demyelinating disease, malignancies of the brain, abscess, encephalitis, autoimmune diseases, or migraine as these conditions may also present WMHs. As the development of the basilar curve is a highly age-related and a long-term process, patients younger than 20 years were also excluded. Based on these criteria we included 290 patients in this study. Written informed consent was obtained from each patient included in the study. The study protocol conformed to the ethical guidelines of the 1975 Declaration of Helsinki and the study protocol had been approved by the Semmelweis University Ethical Committee (TUKEB 264/2019).

3.1.2. Image acquisition

All selected patients had non-contrast brain MRI (Philips Ingenia 1.5T). The protocol contained 3D T1-weighted fast-spin echo, T2-weighted fast field echo and fast spin echo, T2-weighted FLAIR, diffusion weighted imaging and 3D TOF MRI sequences with axial and coronal reconstructions. For our research we used the TOF MRI sequence for vascular reconstruction and the T2-weighted FLAIR MRI sequence for WMH assessment. The main sequence parameters for both sequences can be seen in **Table 1**.

Table 1. Protocols used for T2-weighted FLAIR and Time-of-Flight MRI during image acquisition, Philips Ingenia 1.5T.

Parameter	T2-weighted FLAIR	Time-of-Flight
Slice thickness (mm)	5	1.4
Spacing between slices	6	0.7
Repetition time (msec)	9000	18
Echo time (msec)	140	7
Inversion time (msec)	2450	-
Flip angle (degrees)	90	20
No. of Echoes	162	166
Field of view (mm)	189×230×149	220×199×84
Matrix size	272×162	552×332
Acquisition time (min:sec)	2:15	2:20

3.1.3. Imaging analysis

Image assessment was performed by a single reader blinded to the clinical information. FLAIR images were used to separate patients with and without WMHs into two groups. Separating Deep WMHs from Periventricular WMHs was based on the combination of continuity to the ventricles [43, 44] or if no continuity was seen, a 10 mm distance from the ventricles rule was employed [44].

All patients' brain, who had WMHs were divided with a virtual vertical line in the middle along the falx cerebri creating a right and left side. White matter regions were created on each side along large vessels of interest representing their supplied regions (VA, BA and PCA regions) These regions were identified by means of templates based on imaging and anatomical studies [88] (**Figure 16.** and **Table 2.**).
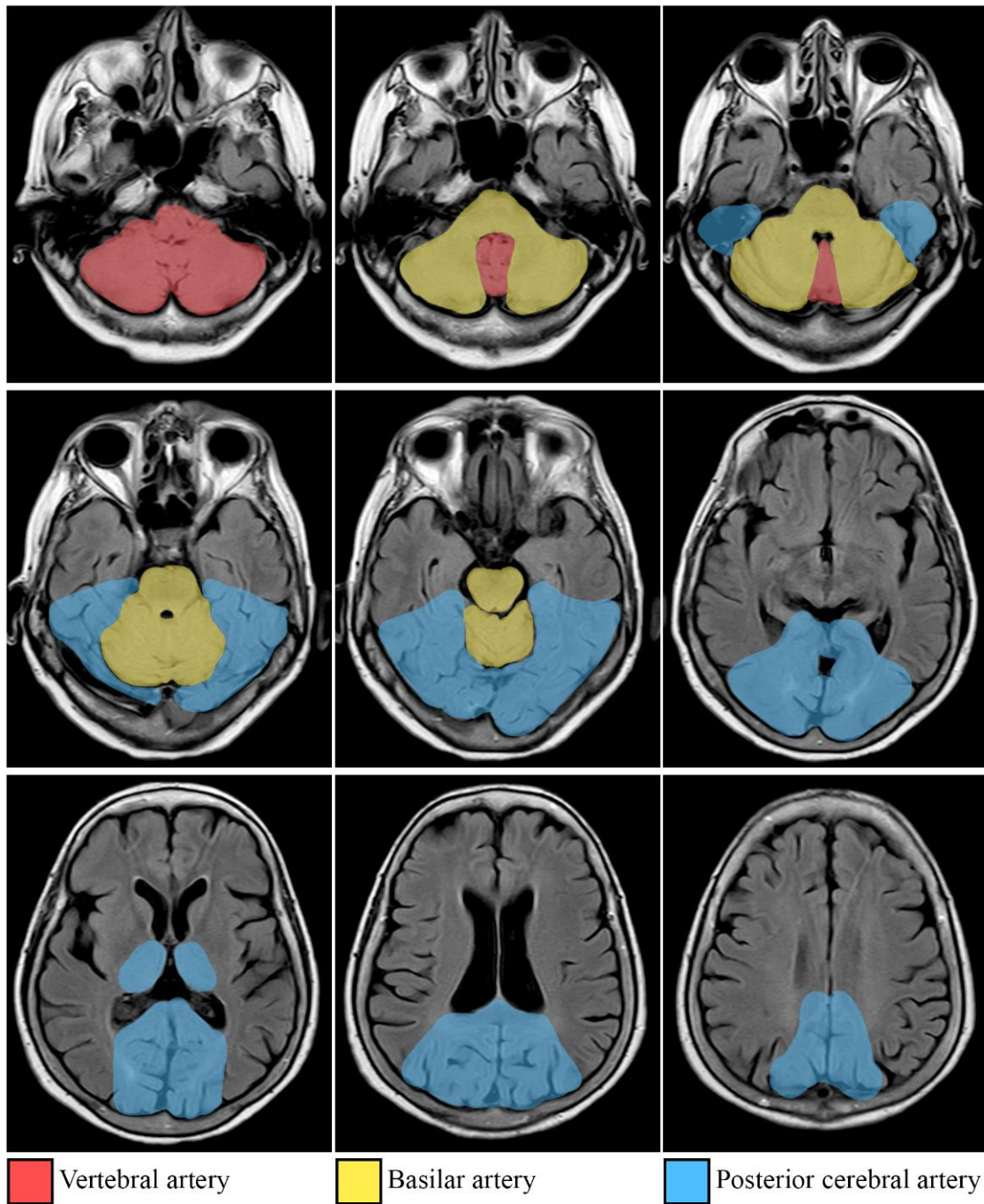
Figure 16.

White matter regions of interest based on posterior circulation arteries which supply blood to the area based on anatomical and imaging templates. (Red) Vertebral artery; (Yellow) Basilar artery; (Blue) Posterior cerebral artery. (Source: Medical Imaging Centre, Semmelweis University, Budapest, Hungary). Own Picture.

Table 2. Regions of interest created with anatomical templates [88] along the vertebral, basilar and posterior cerebral artery. These regions represent the areas these large vessels supply. White matter hyperintensities were analyzed in these regions.

Region	Territories involved
VA region – Vertebral artery	Lower 1/3 of the cerebellum and medulla
BA region – Basilar artery	Upper 2/3 of the cerebellum and pons
PCA region – Posterior cerebral artery	Areas of the parieto-occipital lobe

Each region's WMH burden was compared to its contralateral side. Deep WMH severity classification was based on the age-related white matter changes (ARWMC) score: 0 = no confluence 1 = focal lesions; 2 = beginning confluence; 3 = diffuse involvement of the entire region [45] (**Figure 17.**).
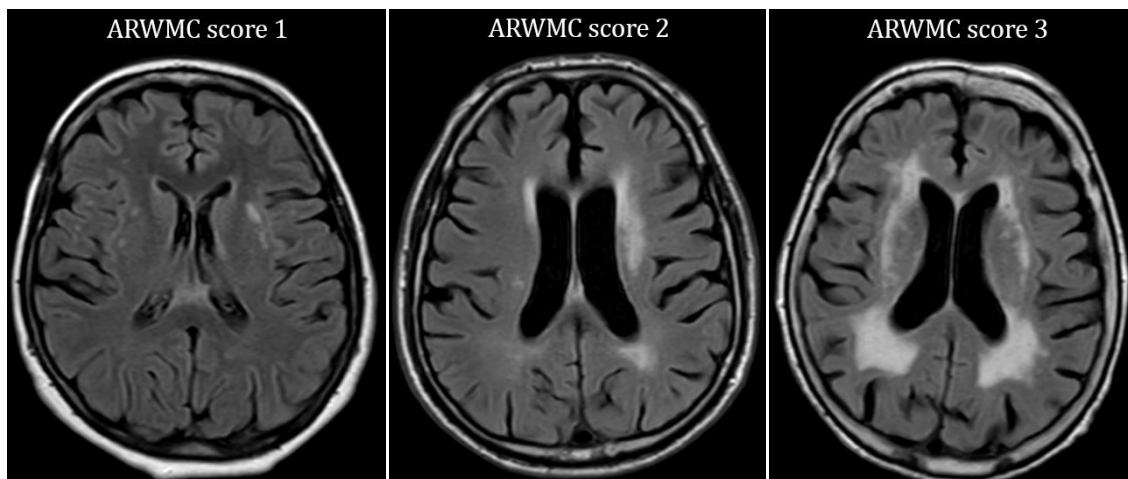
Figure 17.
Deep White matter Hyperintensity severity classification based on the age-related white matter changes (ARWMC) score. (Source: Medical Imaging Centre, Semmelweis University, Budapest, Hungary). Own picture.

The dominant WMH side (laterality) was identified either by higher ARWMC score, or if the score was the same on both sides, by manual counting of the WMH lesions that were ≥5 mm [45]. The posterior communicating arteries were also analyzed. We considered these arteries as hypoplastic or occluded if their external diameter was less than 1 mm, or the arteries were absent [34]. Due to the size of these arteries, it is

difficult to distinguish between hypoplasia, occlusion, or agenesis [34]. For this reason, we categorized these arteries as either detectable or hypoplastic/occluded.

3.1.4. 3D vascular reconstruction and measurements

We used TOF angiography MRI technique to visualize flow within vessels, without the need to administer contrast. To ensure objective, standardized, and semi-automated measurements we used three publicly available software. We used ITK-SNAP (version 3.8.0.) for 3D vascular reconstruction [10], MeshLab (version 2016.12) for post-segmentation editing and cleaning and VMTK (Vascular Modeling Toolkit) for geometry analysis.

First, for all patients we selected the TOF MR images from their Digital Imaging and Communications in Medicine (DICOM) file and imported it into ITK-SNAP. The program previews these images in axial, sagittal and coronal axis. After selecting "Active Contour Segmentation Mode" the volume of interest can be selected on all free planes with a resizable rectangle (**Figure 18.**).
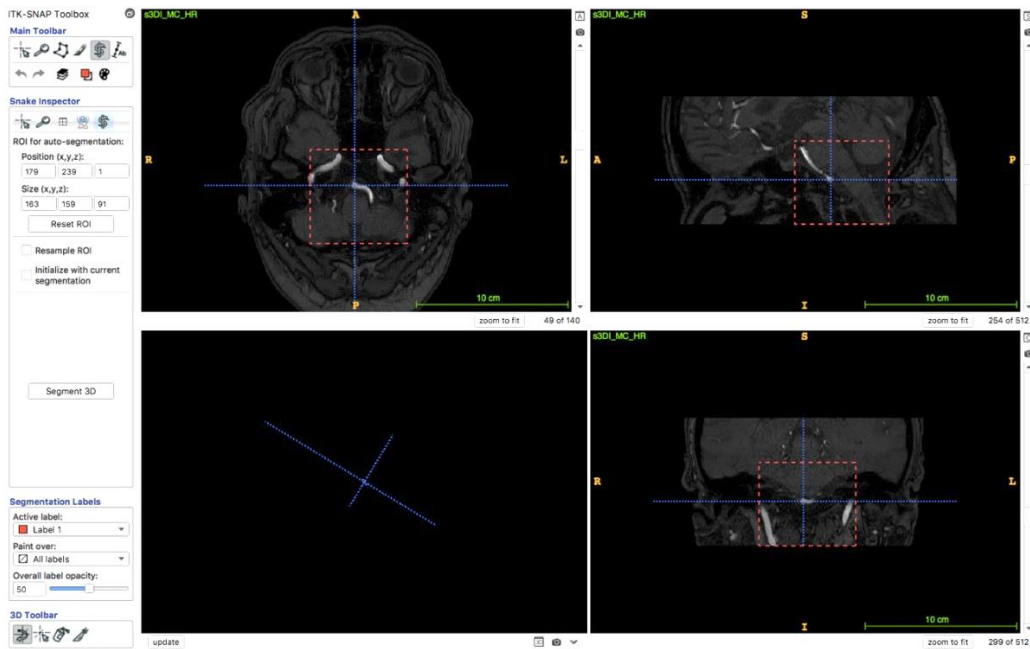
Figure 18.

Selecting the volume of interest for semi-automatic contour segmentation on the axial, coronal and sagittal plain. ITK-SNAP software version 3.8.0. Own picture.

For our research we set the coronal/sagittal starting point to be the beginning of the V4 section of the VA which after a loop runs medial from the C2 foramen transversarium. The ending point is just above the BA top after the branching of the two PCA. On the axial plane we made the rectangle large enough to capture both VAs and the BA on all slices. For segmentation methods ITK-SNAP has four options: thresholding, classification, clustering, and edge attraction. Due to the high contrast observable on TOF MR images between the vessels (high intensity) and the surrounding brain structures (low intensity) we opted to use the thresholding method.   For this method appropriate lower and upper threshold values are set manually (**Figure 19.**).
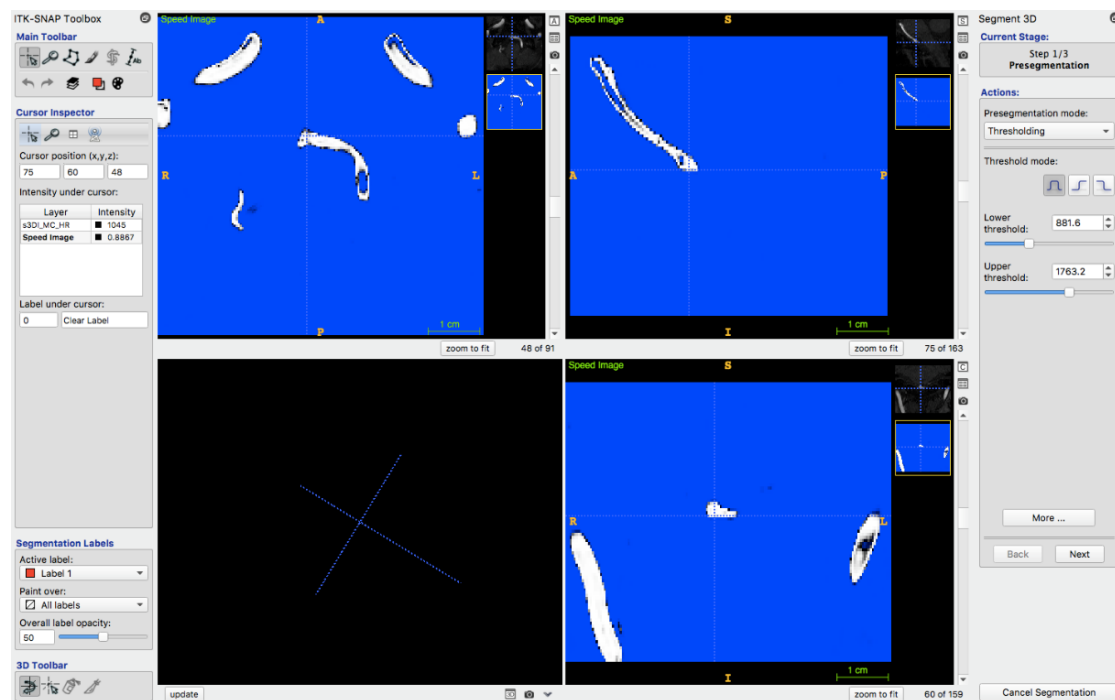
Figure 19.

Setting the lower and upper threshold for the Active Contour Segmentation Mode on Time-of-Flight MRI sequence to minimize artifacts on the final model. ITK-SNAP software version 3.8.0. Own picture.

We used a lower threshold value of approx. 850±50 grey level intensity. Any value lower than this resulted in models including parts of the surrounding cerebellum and brainstem deforming the model and resulting in inaccurate measurements. Any value higher than this resulted in partial reconstructions, usually losing larger parts of

the vertebral arteries. We used a higher threshold of approx. 2500±100 grey level intensity. Lowering the value rarely resulted in minor artefacts due to partial reconstruction of the non-dominant VA. However, setting this value too high greatly increased post processing work as it also included small perforating arteries.

Using the aforementioned threshold values consistently yielded the most accurate models. After this the program requires the user to manually place seed "bubbles" with changeable size along the vessels as reference points for the segmentation (**Figure 20.**).
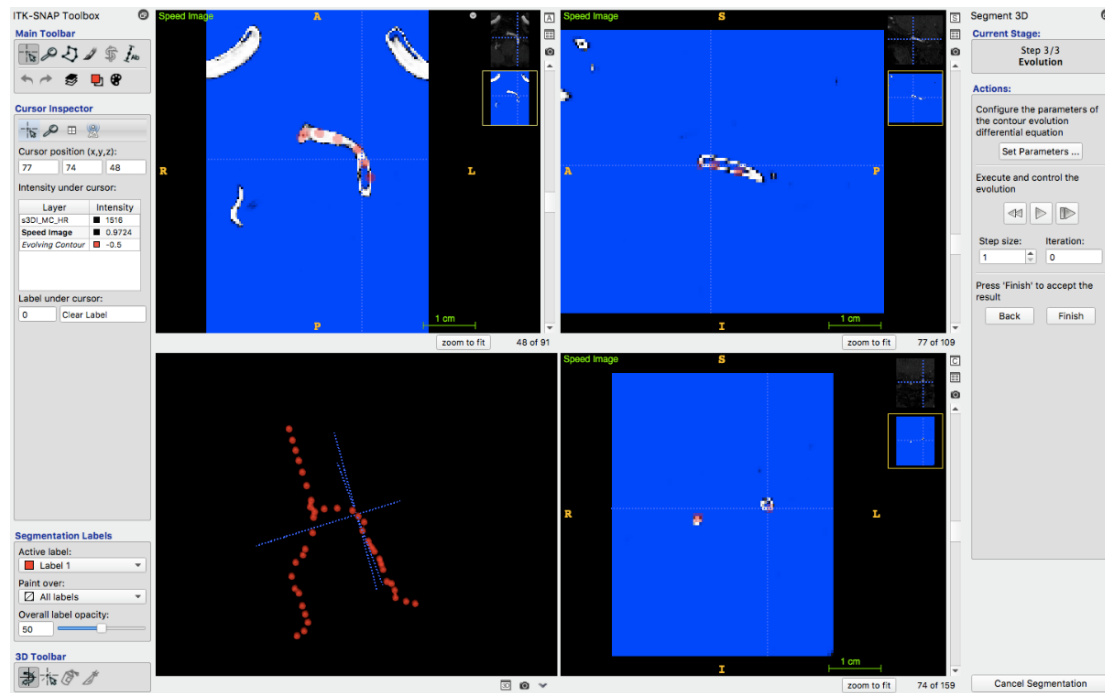
Figure 20.

Manually adding seed "bubbles" with changeable size along the vertebrobasilar system which will be the reference points for the 3D semi-automated segmentation process. ITK-SNAP software version 3.8.0. Own picture.

Subsequently, initiating the segmentation process of the software will create a 3D model of the vertebrobasilar system. At this stage we can continuously preview our 3D model reconstruction process. If we observe any partial reconstruction or high artefact count, we can pause the process and revert to a previous step to fine-tune our

settings (**Figure 21.**).
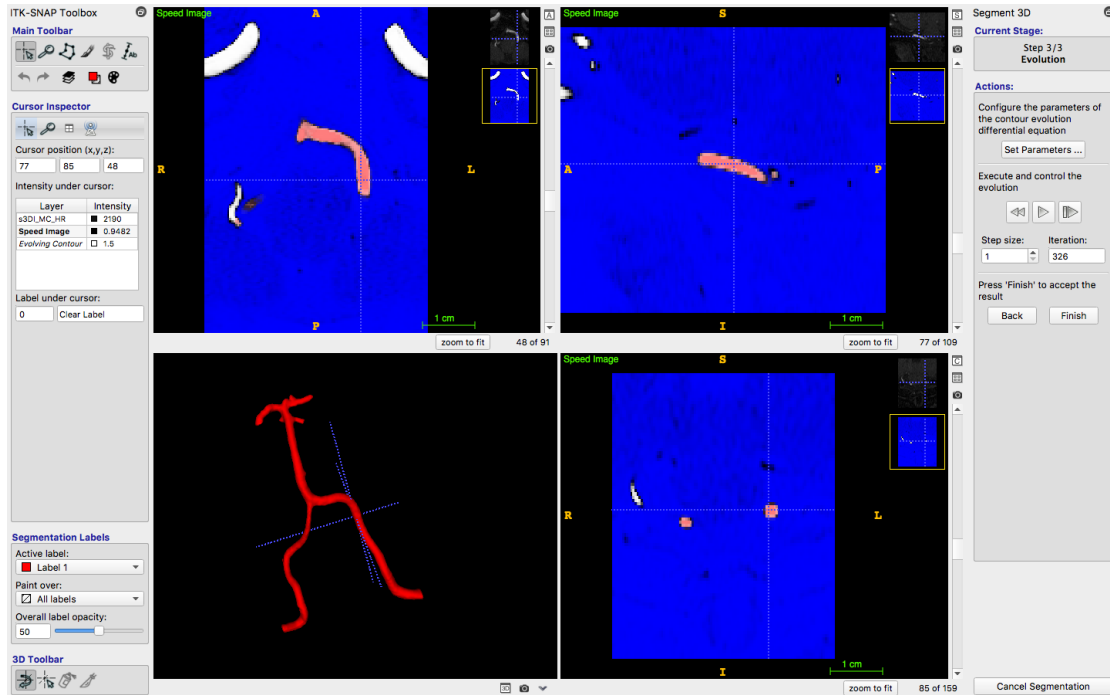
Figure 21.

Completed accurate 3D semi-automated segmentation of the vertebrobasilar system. The model can be previewed in the lower left corner. ITK-SNAP software version 3.8.0. Own picture.

After obtaining an accurate and acceptable reconstruction of the volume of interest we can save the reconstruction in Standard Triangle Language (.stl) format, which is a native file format for most stereolithography computer-aided design software. This creates a surface mesh built entirely from rectangles. The last step is to postprocess the created model for measurement.

For postprocessing all individual 3D mesh models were imported into MeshLab (v2016.12) and smoothed with the Taubin algorithm **[10]**. Both vertebral arteries were cut after the curve around the arc of the atlas. The basilar top (with the two branching PCA and the two superior cerebellar arteries) were also cut under the lower branching superior cerebellar artery with a straight horizontal line. This process ensured obtaining the same sections of the measured arteries (**Figure 22.**).
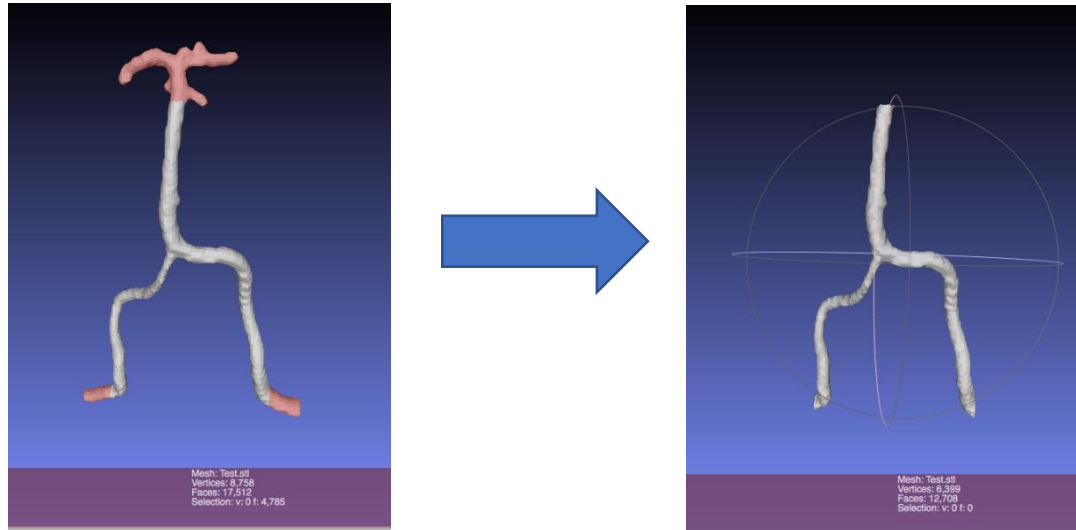
Figure 22.

The 3D reconstructed vertebrobasilar system is imported into MeshLab (v2016.12) for postprocessing (left). The model is smoothed with the Taubin algorithm. The basilar top and the V3 sections of the vertebral arteries are cut (right). Own picture.

The next step was that we created an automated measurement method within the framework of the VMTK application using Python scripts. After locking all models in the same position, in the 3D plane, the program could automatically recognize the left (tan), and right vertebral artery (red), and the basilar artery (blue). This method ensured standardized measurement for each morphological index of the vertebrobasilar system (**Figure 23.**).

Figure 23.

3D reconstructed model of the vertebrobasilar system. After locking all models in the same position, the Vascular Modeling Tool Kit (VMTK) application using Python scripts identifies and measures the left (tan) and right vertebral artery (red) and the basilar artery (blue). Own picture.

We set a difference of 0.3 mm or higher in diameter to define the dominance between the two VAs, which was based on earlier publications assessing vertebral artery diameter difference [66, 73]. Volume, curvature, torsion, and tortuosity was also measured on both VAs. The angle of the vertebrobasilar junction was measured between the two VAs. On the BA, we measured the length, volume, curvature, and cross-section. We further grouped patients based on a two-step process. First, we connected the confluence of the VAs and the basilar top with a straight line. Second, we separated each patient based on if the BA deviated to the left or to the right, while also measuring the extent of the deviation.

3.1.5. Statistical analysis

All analysis were adjusted for age and gender. A descriptive analysis (mean, standard deviation, and percentages) was calculated for the demographic data and the

37

measured morphological indices in R studio (v.1.1.463). The occurrence of comorbidities between the WMH and the control group was analyzed using Fisher's Exact Test. We used Mann-Whitney U test in the analysis of all morphological parameters as they did not show normal distribution. This method tests a general null hypothesis that the distributions of the two examined group are the same. A significant test means that one distribution is stochastically greater than the other, reflecting that there may be differences between the two groups, regarding the examined parameter. VA dominance was analyzed in conjunction with VA region WMH laterality (Fisher's Exact test) and each VA measured parameters (Mann-Whitney U test). The bending direction of the BA was analyzed in conjunction with BA region WMH laterality (Fisher's Exact test) and BA measured parameters (Mann-Whitney U test). We used the Spearman correlation to analyze the directional relationship between VA dominance and the bending direction of the BA. We performed 5 logistic regression analysis for white matter lesions in the PCA regions in SPSS v2.4 to determine variables, that were predictors for WMHs. The 5 logistic regression analysis was based on, whether the posterior communicating artery was occluded, or hypoplastic (both detectable, both hypoplastic/occluded, only left or right hypoplastic/occluded and finally including the whole cohort). Each regression model included VA dominance, bending direction of the BA and all the measured BA parameters. Because of the multiple parameters tested simultaneously, we applied Bonferroni correction for statistical comparisons. When multiple hypotheses are tested the chance of observing a false significant event increases. To compensate for this, we took the desired p value (p<0.05) and divided it with the number of hypotheses tested at the same time. Bonferroni correction then tests each individual hypothesis based on this value. Any p values less than 0.001 are indicated as p<0.001.

3.2. Study 2. Are the Morphological Indices of the Vertebrobasilar System Heritable? A Twin Study Based on 3D Reconstructed Models

3.2.1. Patients

Two hundred healthy Caucasian twins (100 pairs) were randomly selected for our study from the Hungarian Twin Registry [89]. These patients underwent T2-weighted FLAIR and 3D TOF MRI using the same image acquisition protocol from the previous study (**Table 1.** Page 27). The study protocol conformed to the ethical guidelines of the 1975 Declaration of Helsinki and the study protocol was approved by the local Ethical Committees (Semmelweis University TUKEB 189-1/2014, BAZM Hospital Ethical Committee approved on 06 October 2016). All the participants signed an informed consent form. Self-reported questionnaires were used to maximize the accuracy of zygosity classification and to collect a detailed medical history and risk factors [90]. Exclusion criteria consisted of pregnancy, claustrophobia, or intervention in the vertebrobasilar system. We recorded exercise, smoking, alcohol consumption, body weight, height, BMI, hypertension, diabetes, and hyperlipidemia. Former and current smokers were included in the smoking group.

3.2.2. 3D Reconstruction

Each twin underwent the same 3D TOF MRI protocol described in **Table 1.** (Page 30.) (Philips Ingenia 1.5 T). We created a 3D reconstruction of the vertebrobasilar system for each twin based on the TOF MR images. We used ITK-SNAP software's (version 3.8.0.) built in semi-automated segmentation tool for reconstruction described as in section **3.1.4.** (3D vascular reconstruction and measurements). For postprocessing all individual 3D mesh models were imported into MeshLab (v2016.12) and smoothed with the Taubin algorithm [11]. Both vertebral arteries were cut after the V3 section which creates a curve around the arc of the atlas. The basilar top with the two branching PCAs were also cut under the lower branching superior cerebellar artery with a straight horizontal. This method ensured obtaining the same three main arteries for our standardized measurement as in our previous research. The descriptors of the

vertebrobasilar geometry were extracted from the smoothed meshes semi-automatically by using VMTK scripts programmed within a Python environment. After locking all models in the same position in the 3D plane VMTK-based scripts could recognize the left and right VAs along with the BA and provide standardized measurements to analyze the morphological properties of these vessels (**Figure 24.**).
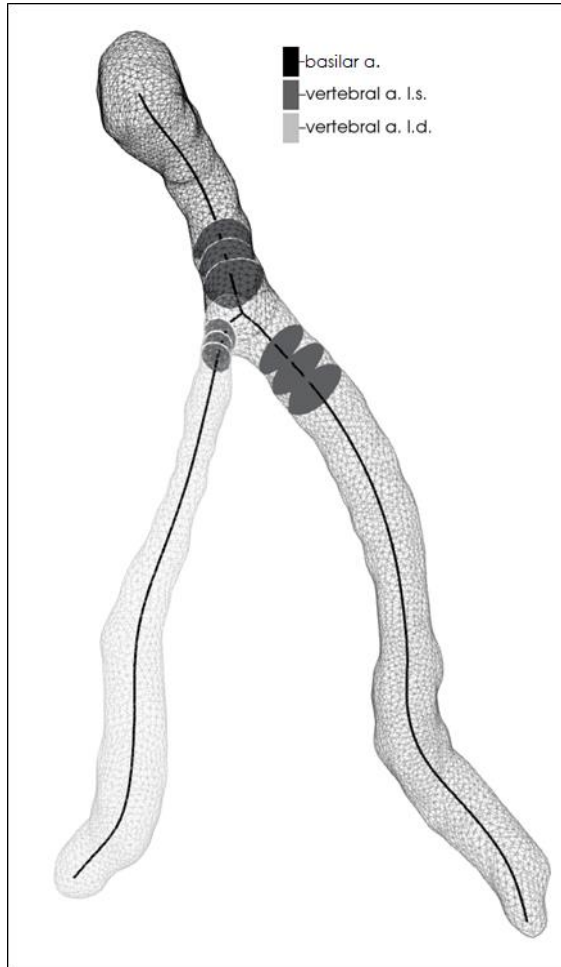
Figure 24.

Visual representation of our written software analyzing the vertebrobasilar reconstruction of a patient. The program identifies the arteries based on the confluence of the two vertebral arteries in a fixed position. The program creates the centerline for each vessel and measures the different geometrical indices. Own picture.

To eliminate artefact-based differences and to identify the dominant VA, a difference higher than 0.3 mm was set based on earlier publications [66, 73]. The cross-sectional area, curvature, torsion, and tortuosity were measured on both vertebral arteries. The VA curvature was defined as the inverse of the radius of the local osculating circle along the centerline of the vessel and VA torsion as the amount by which the osculating plane rotates along the centerline. VA tortuosity was defined as the centerline length of the vessel divided by the shortest distance between the start and the

end of the vessel. On the BA, we measured the length, volume, curvature, and cross-sectional area. The bending direction of the BA was measured with a 2-step process. First, we connected the confluence of the two VAs and the basilar top with a straight line. Second, we measured the median deviation from this straight line on the X axis. BA torsion and tortuosity was also measured.

3.2.3. Statistical analysis

A descriptive analysis (mean, standard deviation, and percentages) for the risk factors and vertebrobasilar parameters was calculated with SPSS Statistics v2.4. ACE univariate genetic modeling was performed with the RStudio version 1.3.1093 and OpenMx 2.18. The phenotypic variance of the different morphological parameters was decomposed into heritability (A), shared (C), and unshared (E) environmental effects (ACE analysis). A heritability estimate was calculated using within-pair correlation between MZ and DZ twins with 95% confidence intervals (CI). We compared the saturated model (correlation matrix without zygosity) and the ACE model (correlation matrix including zygosity) for each parameter. If the two model greatly differed the results were considered only as informative. To investigate whether the anthropometric or cardiovascular risk factors influenced the morphological indices beyond age and sex, bivariate regression analyses were performed. Based on these regression models, covariates were added to further adjust the heritability models (Model 1 and Model 2). For each morphological phenotype, Model 1 was only adjusted for age and sex, while Model 2 was additionally corrected for all the risk factors with significant relationship. The best fitting ACE models were chosen based on comparing 2*log-likelihoods and on the Akaike and Bayesian information criterion (AIC and BIC). 2*log-likelihood describes how well a model fits the data and usually are compared between two models to get the better fitting model. While AIC and BIC are derived from the 2*log-likelihood and measures a model's degree of freedom and the number of parameters included in the model. AIC and BIC both increases if more parameters are added into the model. Both parameter favors the less complicated and the better fitting model.

4. RESULTS

4.1. Study 1. Laterality of deep white matter hyperintensity correlates with basilar artery bending and vertebral artery dominance

290 patients with TOF and FLAIR MRI sequences were involved (**Table 3.**). The average age of the whole cohort was 52.4±17.6 years and 59.3% of them were female (118 male / 172 female). The WMH group consisted of 204 patients (average age was 57.6±16.7 years; 57.8% female) and the control group consisted of 86 patients (average age 40.2±13.0 years, 62.0% female). The median age of the WMH group were significantly higher ($\tilde{x}$=62) compared to the control group ($\tilde{x}$=37, p<0.001 - Mann-Whitney U test). Both hypertension and diabetes were significantly more common in the WMH group compared to the control group (p=0.004, OR= 8.75 and p<0.001, OR= 4.08, respectively - Fisher's Exact test).

Table 3. General demographic data and risk factors between our different groups.

	Whole Cohort	Control group	Deep WMH group
	(n=290)	(n=86)	(n=204)
General demographic data			
Age (year, Mean±SD)	52.4	40.2	57.6
Sex (Male:Female)	118 : 172	32: 54	86 / 118
Risk factors (n)			
Hypertension	126	11 (8.73%)	115 (91.26%)
Diabetes	38	4 (10.52%)	34 (89.47%)
Hyperlipidemia	18	4 (22.22%)	14 (77.78%)
Basilar artery length (mm)	24.2	22.74	24.87
Basilar artery diameter (mm)	3.61	3.54	3.67
Basilar artery area (mm²)	10.56	10.04	10.81
Basilar artery volume (mm³)	256.93	229.32	269.73

	Whole Cohort	Control group	Deep WMH group
BA deviation from centerline (mm)	2.03	1.43	2.29
Basilar artery tortuosity (%)	7.17%	5.05%	8.15%
Basilar artery torsion (%)	15.32%	14.57%	15.67%
Left vertebral artery diameter (mm)	2.87	2.81	2.90
Right vertebral artery diameter (mm)	2.68	2.66	2.69
VA dimension difference (mm)	0.76	0.69	0.79
Vertebral artery angle (°)	66.16	66.03	66.22
Left vertebral artery curvature (%)	12.31%	11.97%	12.47%
Right vertebral artery curvature (%)	12.83%	12.42%	13.02%
Left vertebral artery tortuosity (%)	12.92%	9.76%	14.39%
Right vertebral artery tortuosity (%)	11.03%	8.23%	12.32%
Left vertebral artery torsion (%)	13.86%	13.46%	14.04%
Right vertebral artery torsion (%)	12.73%	17.87%	10.03%

As expected, left VA dominance was more common (**Table 4.**). In contrast, vertebra artery curvature ($\tilde{x}=0.15$, $p<0.001$ - Mann-Whitney U test) and torsion ($\tilde{x}=4.9$, $p=0.002$ - Mann-Whitney U test) was significantly higher in the non-dominant VA. We found that the VA region WMH burden was significantly higher on the non-dominant hemisphere of the VA ($p=0.006$, OR=0.13 - Fisher's Exact test). VA angles were similar between groups WMH/Control and Left dominant/Right dominant VA. 66 patients had less than 0.3 mm difference between the two vertebral artery cross-section and were classified as even. These patients showed no correlation with cerebellar WMH laterality.

Table 4. Laterality of dominant vertebral artery.

	Whole Cohort	Control group	Deep WMH group
	(n=290)	(n=86)	(n=204)
Side of dominant vertebral artery			
Right side (>0.3mm difference)	84	26	58
Left side (>0.3mm difference)	139	39	100
Classified as even	66	20	46

VA dominance and bending direction of the BA correlated inversely (p<0.001, r=-0.56 - Spearman correlation), which has already been reported in previous publications [10, 66]. There were 3 times more patients with the right bending BA and left dominant VA in the whole cohort (**Table 5.**). We found that the tortuosity ($\tilde{x}$=0.05%, p=0.019 - Mann-Whitney U test), the length ($\tilde{x}$=24.13, p=0.005 - Mann-Whitney U test) and mean cross-sectional area of the BA ($\tilde{x}$=10.73, p=0.007 - Mann-Whitney U test) were significantly higher in the WMH group. BA region WMH dominance was significantly higher on the opposite side of the BA curve (p=0.002, OR=0.06 - Fisher's Exact test).

Table 5. Bending direction of the basilar artery between our different groups.

	Whole Cohort	Control group	Deep WMH group
	(n=290)	(n=86)	(n=204)
Bending direction of the BA			
Right curve	143	36	107
Left curve	41	7	34
Classified as even	106	43	63

Logistic regression which included the whole cohort showed age (b=0.56, p<0.001, OR=1.06) and hypertension (b=1.33, p<0.001, OR=1.23) as predictors for PCA region WMH burden severity. From the 290 patients: 72 patients' posterior communicating artery was detectable on both sides (25%), 56 patients (19%) had left hypoplastic/ occluded and 67 patients (23%) had right hypoplastic/occluded posterior communicating arteries. 95 patients (33%) had hypoplastic/occluded posterior communicating arteries on both sides. Out of these 95 patients 73 had WMHs in the PCA regions. Logistic regression including the aforementioned 73 patients revealed basilar deviation from the centerline (b=0.316, p=0.013, OR=1.37) as a predictor for PCA region WMH laterality.

4.2. Study 2. Are the Morphological Indices of the Vertebrobasilar System Heritable? A Twin Study Based on 3D Reconstructed Models

In this study, of the 200 twins (100 pairs), 134 were MZ (67 pairs) and 66 were DZ (33 pairs). The average age was 49.6 (SD: ±14.4) and 56.0 (SD: ±15.2) years in the MZ and DZ groups, respectively. The two groups were significantly different in age (p = 0.004). The male to female ratio was 44:90 (67% female) in the MZ group and 23:43 (65% female) in the DZ group. No significant difference was observed between the MZ and DZ groups regarding anthropometric variables and risk factors. **Table 6.** shows the risk factors and the measured characteristics of our population.

Table 6. Demographic, clinical characteristics, and vessel morphological measurements by zygosity. *: Indicates a significant difference between the mono- and dizygotic groups. BMI: body mass index; MZ: Monozygotic; DZ: Dizygotic.

	Total	MZ	DZ	*p*
Zygosity (*n* pairs)	100	67	33	-
Age	51.66	49.57	56	0.004 *
Sex (F:M)	132:67	90:44	43:23	-

	Total	MZ	DZ	*p*
Does weekly exercise	63.00%	68.65%	51.51%	0.02 *
Alcohol consumption once a week	54.00%	52.23%	59.09%	0.29
Ever Smoked	27.00%	28.35%	24.24%	0.60
Height (cm)	167.95	167.90	168.05	0.91
Weight (kg)	72.75	72.52	73.22	0.74
BMI (kg/m^2)	25.74	25.56	26.12	0.41
Diagnosed with diabetes	8.50%	9.70%	6.06%	0.41
Diagnosed with hypertension	30.50%	30.60%	30.30%	0.95
Diagnosed with dyslipidemia	24.50%	24.62%	24.24%	0.97
Basilar artery length (mm)	24.08	23.77	24.73	0.14
BA diameter (calculated mm)	3.42	3.39	3.49	0.23
Basilar artery area (mm²)	9.43	9.23	9.84	0.17
Basilar artery volume (mm³)	218.28	210.47	234.49	0.05
Basilar artery curvature (mm)	2.57	2.51	2.68	0.06
Basilar artery tortuosity (%)	6.37%	6.03%	7.08%	0.35
Basilar artery torsion (%)	11.29%	10.59%	12.57%	0.19
Left vertebral a. diameter (mm)	2.44	2.44	2.45	0.92
Right vertebral a. diameter (mm)	2.36	2.36	2.36	0.91
VA dimension difference (mm)	0.75	0.71	0.82	0.22
Left vertebral artery curvature (%)	7.79%	7.88%	7.61%	0.42
Right vertebral artery curvature (%)	8.10%	8.14%	8.04%	0.77
Left vertebral artery tortuosity (%)	11.77%	11.12%	13.10%	0.23
Right vertebral artery tortuosity (%)	11.57%	10.71%	13.35%	0.07
Left vertebral artery torsion (%)	12.34%	12.64%	11.73%	0.51
Right vertebral artery torsion (%)	12.62%	12.75%	12.35%	0.78

Table 7. shows age- and sex-adjusted parameter estimates for additive genetic (A), common environmental (C), and unique environmental influences (E) on the different measured parameters by structural equation modeling. The within-pair correlation in MZ twins was higher than in DZ for the BA length (0.616 vs. 0.288) and BA volume (0.646 vs. 0.016).

The age- and sex-adjusted additive genetic effect, within the most parsimonious model, accounted for 63% (95% CI: 45.7–75.2%) of the variance of the BA length and 60.1% (95% CI: 42.4–73.2%) of the variance of the BA volume. Unshared environmental effects accounted for 37% (95% CI: 24.8–54.3%) of the variance of the BA length and 39.9% (26.8–57.6%) of the variance of the BA volume.

Although the within-pair correlation was higher in MZ twins than DZ for the VA diameter difference, left and right VA tortuosity, the ACE model differed significantly for these parameters from the saturated model, therefore, these results were only informative. The right VA curvature was moderately influenced by additive genetic factors (21%; 95% CI: 0–42.1%), and it was highly determined by the unshared environment (78.4%; 95% CI: 57.2–100%).

No heritability was found for the rest of the measured parameters. There was no within-pair correlation for either MZ and DZ twins for the left and right VA torsion, therefore, the majority of the variances could be attributed to unshared environmental effects.

Table 7. Age- and sex-adjusted estimates for genetic (A), shared environmental (C), and unshared environmental (E) influence on the different measured parameters by structural equation modeling (95% confidence intervals). The most parsimonious, univariate structural equation model estimates are marked with *and highlighted as bold. BA: basilar artery; VA: vertebral artery; *r*: Intrapair correlation; MZ: Monozygotic; DZ: Dizygotic.

	Model	A	95% CI	C	95% CI	E	95% CI
BA length (mm)	A-C-E	0.63	0.457–0.752	0	0–0.445	0.37	0.248–0.543
rMZ: 0.616 (0.434 0.749)	**A-E ***	0.63	0.457–0.752			0.37	0.248–0.543
rDZ: 0.288 (−0.048 0.566)	C-E			0.503	0.331–0.641	0.497	0.359–0.669
BA area (mm²)	A-C-E	0.13	0–0.571	0.252	0–0.513	0.618	0.426–0.827
rMZ: 0.361 (0.127 0.558)	A-E	0.409	0.192–0.585			0.591	0.415–0.808
rDZ: 0.346 (0.02 0.606)	**C-E ***			0.354	0.168–0.516	0.646	0.484–0.832
BA volume (mm³)	A-C-E	0.601	0.255–0.732	0	0–0.292	0.399	0.268–0.576
rMZ: 0.646 (0.474 0.771)	**A-E ***	0.601	0.424–0.732			0.399	0.268–0.576
rDZ: 0.016 (−0.316 0.347)	C-E			0.452	0.281–0.596	0.548	0.404–0.719
BA curvature (mm)	A-C-E	0	0–0.371	0.164	0–0.347	0.836	0.653–1
rMZ: 0.117 (−0.133 0.354)	A-E	0.174	0–0.388			0.826	0.612–1
rDZ: 0.231 (−0.098 0.514)	**C-E ***			0.164	0–0.347	0.836	0.653–1
BA tortuosity (%)	A-C-E	0.099	0–0.627	0.395	0–0.618	0.507	0.345–0.699
rMZ: 0.492 (0.275 0.663)	A-E	0.515	0.32–0.664			0.485	0.336–0.68
rDZ: 0.464 (0.162 0.686)	**C-E ***			0.475	0.297–0.621	0.525	0.379–0.703
BA torsion (%)	A-C-E	0	0–0.239	0	0–0.196	1	0.761–1
rMZ: −0.003 (−0.246 0.241)	C-E			0	0–0.196	1	0.804–1
rDZ: −0.016 (−0.345 0.317)	**E ***					1	1
Left VA diameter (mm)	A-C-E	0.003	0–0.436	0.229	0–0.412	0.768	0.563–0.965
rMZ: 0.255 (0.011 0.473)	A-E	0.249	0.03–0.445			0.751	0.555–0.97
rDZ: 0.213 (−0.124 0.506)	**C-E ***			0.232	0.035–0.412	0.768	0.588–0.965

	Model	A	95% CI	C	95% CI	E	95% CI
Right VA diameter (mm)	A-C-E	0.181	0–0.601	0.257	0–0.559	0.562	0.39–0.765
rMZ: 0.454 (0.236 0.629)	A-E	0.453	0.254–0.612			0.547	0.388–0.746
rDZ: 0.339 (0.016 0.598)	**C-E ***			0.41	0.228–0.564	0.59	0.436–0.772
VA difference (mm)	A-C-E	0.23	0–0.444	0	0–0.29	0.77	0.556–1
rMZ: 0.306 (0.064 0.514)	**A-E ***	0.23	0–0.444			0.77	0.556–1
rDZ: −0.089 (−0.405 0.248)	C-E			0.144	0–0.335	0.856	0.665–1
Left VA curvature (%)	A-C-E	0.064	0–0.522	0.274	0–0.494	0.662	0.474–0.858
rMZ: 0.349 (0.116 0.547)	A-E	0.358	0.148–0.535			0.642	0.465–0.852
rDZ: 0.284 (−0.061 0.567)	**C-E ***			0.329	0.139–0.495	0.671	0.505–0.861
Right VA curvature (%)	A-C-E	0.216	0–0.428	0	0–0.292	0.784	0.572–1
rMZ: 0.27 (0.027 0.483)	**A-E ***	0.216	0–0.428			0.784	0.572–1
rDZ: −0.066 (−0.381 0.263)	C-E			0.141	0–0.327	0.859	0.673–1
Left VA tortuosity (%)	A-C-E	0.339	0–0.635	0.124	0–0.522	0.536	0.365–0.769
rMZ: 0.409 (0.185 0.594)	**A-E ***	0.476	0.263–0.638			0.524	0.362–0.737
rDZ: 0.349 (0.018 0.611)	C-E			0.386	0.2–0.545	0.614	0.455–0.8
Right VA tortuosity (%)	A-C-E	0.557	0.043–0.711	0	0–0.391	0.443	0.289–0.659
rMZ: 0.477 (0.248 0.655)	**A-E ***	0.557	0.341–0.711			0.443	0.289–0.659
rDZ: 0.281 (−0.048 0.556)	C-E			0.385	0.199–0.544	0.615	0.456–0.801
Left VA torsion (%)	A-C-E	0.057	0–0.271	0	0–0.23	0.943	0.729–1
rMZ: 0.078 (−0.167 0.316)	C-E			0.039	0–0.233	0.961	0.767–1
rDZ: −0.06 (−0.395 0.292)	**E ***					1	1
Right VA torsion (%)	A-C-E	0	0–0.168	0	0–0.186	1	0.814–1
rMZ: −0.1 (−0.336 0.149)	C-E			0	0–0.186	1	0.814–1
rDZ: 0.225 (−0.104 0.512)	**E ***					1	1

The final ACE models were corrected for age, sex, sport activity, alcohol, smoking, diabetes, hypertension, dyslipidemia, height, weight, and BMI. We constructed models where we only corrected for age and sex and compared the two types of models for all the examined variables. **Table 8.** shows the variables where there was a significant difference between the models.

Table 8. Significant differences between the variables after correcting the final ACE models for age, sex, sport activity, alcohol, smoking, diabetes, hypertension, dyslipidemia, height, weight, and BMI. -2LL_base: -2*Loglikelihood of the model containing all the variables, -2LL_reduced: -2*Loglikelihood of the model containing only age and sex, p: P-value of the likelihood ratio test; VA: vertebral artery.

	-2LL_Base	-2LL_Reduced	p
Basilar area	242.4058	280.1872	<0.001
Basilar volume	360.3536	401.4033	<0.001
Basilar diameter	292.5449	330.3450	<0.001
Left VA curvature	22.15288	37.39575	0.05
Right VA curvature	12.94010	39.96847	<0.001
Left VA diameter	418.4466	435.5442	0.03
Basilar length	1144.393	1165.349	0.01

From the fitted ACE models, we identified several significant environmental variables in our models, and two of them (smoking, height) were consistent across similar variables, therefore, we could conclude that smoking and height had a significant effect on the dimensions of the BA, and smoking may also affect the VA (we could only fit the ACE model on the left VA, therefore, we do not have regression data about the right side) (**Table 9.**).

Table 9. Smoking and height were consistent across similar variables and showed a significant effect on the dimensions of the basilar artery, while only smoking affects the vertebral artery.

Model	Smoking (Binary)	Height (cm)
Left VA diameter	0.22 (0.002, 0.435)	Not significant
Basilar diameter	0.212 (0.049, 0.375)	0.025 (0.012, 0.037)
Basilar volume	Not significant	0.03 (0.015, 0.045)
Basilar area	0.188 (0.043, 0.332)	0.022 (0.011, 0.033)
95% confidence intervals in the parenthesis		

We should note that a few of our environmental variables did correlate (**Figure 25.**). Therefore, it is possible, that in a few cases we could not show significant effects, when in reality they may exist due to multicollinearity.
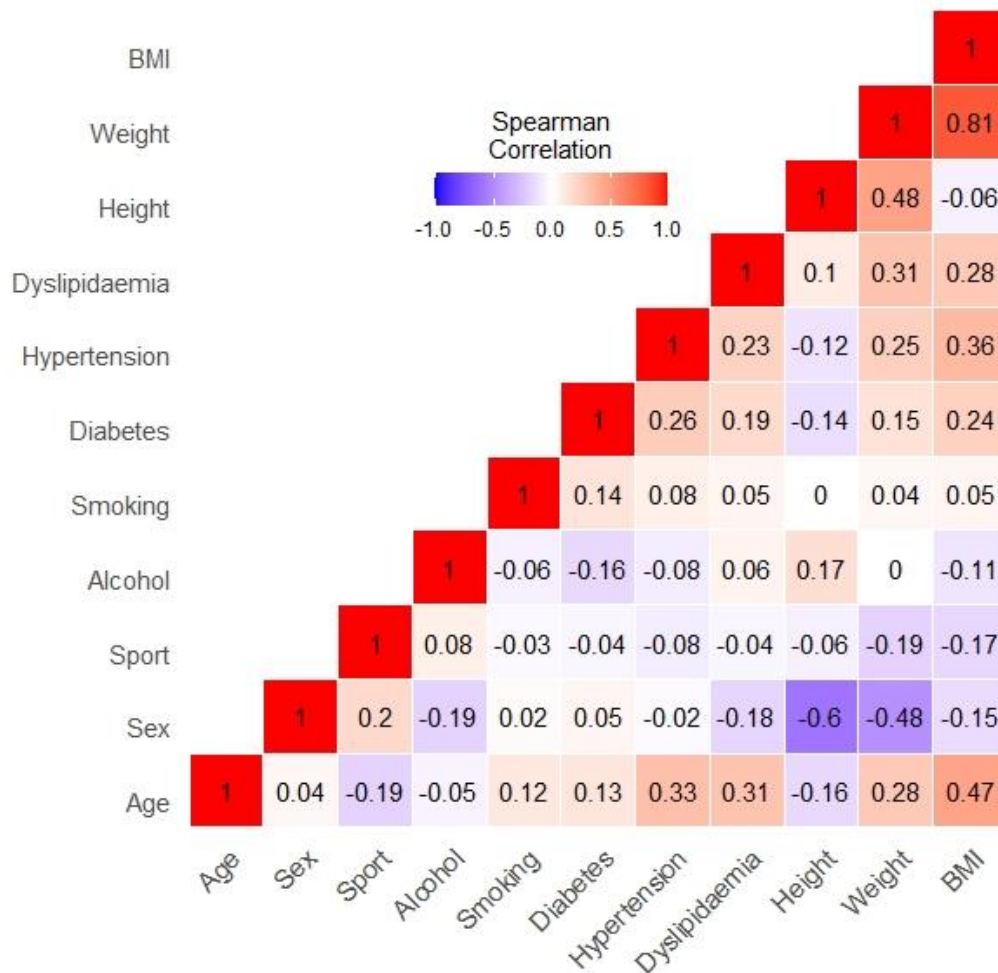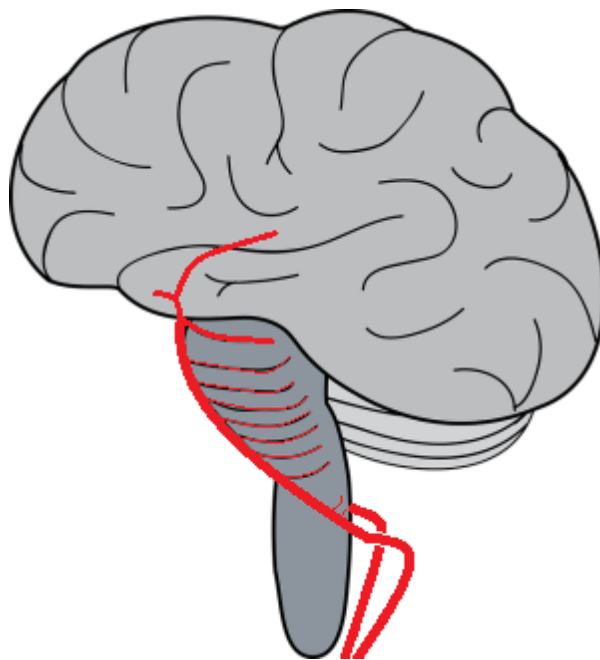

Figure 25.

Spearman correlation table of the investigated risk factor and the measured characteristics of our population made with RStudio (version 1.3.1093). BMI: body mass index. Own picture.

5. DISCUSSION

The aim of our clinical study was to investigate whether WMHs of the posterior brain regions, seen on T2-weighted FLAIR MR images, are influenced by the morphological properties of the vertebrobasilar system. These WMHs have been linked to stroke as a risk factors [41, 42]. Although the relationship between VA dominance and the bending direction of the BA has already been researched, most of these studies focused on the connection with stroke and post-stroke outcomes [69, 82]. As expected, the left VA was more dominant, which can be linked to the fact that the left subclavian artery branches directly from the aortic arch [91]. Our results show that one side VA hypoplasia leads to BA bending of the opposite direction which was consistent with previous reports [69]. This may be explained with inconsistent WSS on the vessel wall caused by asymmetrical blood flow over decades. These effects can lead to increased risk for atherosclerosis on the small curve of the BA [10]. Patients in the WMH group had BAs with increased length, tortuosity, and volume, which was also observed in patients with dolichoectasia [92]. This is in accordance with the observation that among all the intracranial arteries, the BA shows concentric intimal thickening and elastin loss, all of which point toward a predisposition to dilatation and as such has the highest prevalence of dolichoectasia amongst all the intracranial arteries [93]. Intracranial arterial dolichoectasia can be defined, as an increased diameter (Ectasis) and/or long and tortuous course (Dolichos) of at least one cerebral artery, and is considered as an independent risk factor for stroke [94]. However, to be classified as dolichoectasia the diameter of the basilar artery has to be more than 4.5 mm and all of our patients were below this criteria [95]. Our results showed that age and the occurrence of hypertension and diabetes were significantly higher among WMH patients which was in accordance with previous studies [39]. The average age of WMH group patients was 57.6±16.7 years. At this age range, approximately 20-55% of the population has WMH lesions which can go up to almost 100% by the age of 90 [38]. Strassburger et. al. showed that hypertensive patients had significantly higher WMH burden compared to normotensive age-matched patients [96]. These hyperintense lesions are either caused by small subcortical infarcts or more often by a process called incomplete infarction, reflecting chronically reduced blood flow caused by morphological changes in vessels and

arteriolosclerosis [79]. We found a significantly higher VA region WMH burden, increased vessel curvature, and torsion on the non-dominant side of the VA. Different VA flows have been linked to posterior inferior cerebellar artery territory infarctions on the hemisphere of the non-dominant VA [66, 69, 73]. BA region WMH burden was higher on the opposite side of the bending direction of the BA. The causation of this might be the lower blood perfusion in the perforating arterioles branching from the small curve of the basilar artery or that a micro-thrombi formed on atherosclerotic plaques (**Figure 26.**).

Figure 26.

Lateral perforating arterioles of the basilar artery. Own picture.

BA bending has also been linked to pontine infarction on the opposite hemisphere as the BA curve [66, 69, 73]. Zhang et al. identified a BA curvature greater than 3.77 mm as an independent risk factor for pontine infarction [73]. These findings suggest that there might be a stronger etiological connection between subtentorial WMHs and manifested strokes in these regions. WMH severity has been linked to increased risk of stroke and higher cognitive decline after stroke [42]. Jeerakathil et. al. found a strong relationship between the Framingham Stroke Risk Profile (FSRP) and its component risk factors and WMH [83]. A study by Fu et. al. showed that patients with

high WMH burden had increased risk of deep subcortical stroke and a higher risk of recurrent stroke but did not assess whether the laterality of WMHs correlated with the laterality of the patient's stroke [81]. In our investigation we assessed WMH severity in each region with the ARWMC scale and compared it with BA curvature and VA diameter but did not find any connections.

In the PCA regions logistic regression involving all 290 patients identified, as expected, age and hypertension as independent risk factors, however, none of the basilar morphological indices showed significance for the severity of the white matter hyperintensities. This could be explained with the posterior communicating arteries providing anastomoses to the vertebrobasilar system and decreasing the effects of the BA morphology. After selecting patients, with both posterior communicating artery hypoplastic/occluded, logistic regression showed BA deviation from the centerline as risk factor for WMH laterality. We hypothesize that in these cases the BA may supply the majority of blood for the two PCAs [97]. Furthermore, the bending direction of the BA may create an asymmetrical perfusion in the two PCAs.

In our twin study we investigated the heritability of the different vertebrobasilar morphological indices. Our research group has already investigated VA diameter difference and heritability [75], however that study utilized ultrasound as imaging technique and only investigated the V1 and V2 segments of the vessel. Our hypothesis was that most of the measured vertebrobasilar parameters are influenced by genetic factors, which we based on our previous findings [75]. To the best of our knowledge, this was the first twin study that measured the heritability of morphological indices of the intracranial vertebrobasilar system. We demonstrated that the length and volume of the BA is genetically determined, but the role of unique environmental effects remain an important factor. Furthermore, the right VA curvature was only partly genetically influenced, but was greatly impacted by unshared environmental effects. The remaining measured anthropometric indices were affected by shared and unshared environmental effects.

VA difference in diameter and VA hypoplasia are common anatomical variations that can be found on MRI scans [91]. VA difference in diameter can increase the risk of cerebellar ischemic stroke [66, 69]. The hemodynamic mechanism of the

ischemic stroke in patients with increased VA diameter difference is not yet completely understood, but embolization, caused mainly by atherosclerosis seems to be a predisposing factor [91, 98]. The smaller caliber size of the non-dominant VA may result in a lower blood flow and irregular WSS in the BA, which increases the risk of prothrombotic or atherosclerotic processes leading to increased curvature, stenosis, or occlusion [98, 99]. Hong et al. found that amongst posterior inferior cerebellar artery infarction patients, 72.7% of these lesions occurred on the non-dominant side of the VA [66]. Our results show that the V4 section of the VA on both sides was mainly influenced by shared and unshared environmental factors. In contrast, our research group previously in 2017 demonstrated that the diameter of the V1 and V2 segments of the VA on ultrasound was moderately heritable [75]. This difference may arise from the fact that the V4 segment of the VA is more distal from the heart, decreasing the effects of hemodynamic secondary flows in the V4 segment [24]. However, our results also showed that the right-side VA curvature was moderately heritable. This could be, in theory, explained with a lower flow on the right side due to it not directly branching off the aortic arch and thus having lower but more consistent WSS and flow velocities. Yuan et al. found that the asymmetry and variance of the V1-V2 segments are less common compared to the V4 segments [100]. Wake-Buck et al. identified VA curvature and orientation at the two VA's confluence as important factors affecting blood flow velocities based on computational fluid dynamics modeling **[10]**. It has been shown that the uneven VA flow may cause curving and elongation of the BA [7]. The BA length and bending direction has also been linked to increased risk for pontine and thalamic ischemic stroke [6,7]. BA curvature showed a high unshared environmental effect (83.6%; 95% CI: 0.633–1). These findings are in line with previous studies, which suggested that hemodynamic changes caused by lifestyle and comorbidities such as hypertension and diabetes along with VA difference in diameter are the main cause of BA bending. Jeong et al. demonstrated that patients with deep pontine lacunar infarcts were older, had a bigger VA difference in diameter, and measured higher BA angulations [68]. Zhang et al. found similar trends and an added history of hypertension, smoking, high homocysteine, high cholesterol, and type 2 diabetes as risk factors for pontine infarction in patients with increased BA curvature [73]. We found that smoking affected the dimension of the BA, however diabetes, hypertension, and dyslipidemia did

not correlate significantly. Kwon et al. found that among the patients diagnosed with pontine infarcts, the BA volume was higher in paramedian pontine infarcts ($p = 0.016$), while the BA length was higher in lacunar pontine infarcts ($p = 0.034$) [101]. Our results showed that the BA length and volume was moderately heritable. This may be in part explained by the outcome of recent brain volume twin studies, in which Zhao et al. found high brainstem volume heritability [102]. Our hypothesis is that under normal anatomical circumstances, the basilar artery volume and length would increase along with an individual's brainstem volume, but also be affected by hemodynamic disturbances caused by shared and unshared environmental factors. However, further studies are needed to elucidate if there is an overlap between the heritability of brainstem volume and BA length and volume phenotypes.

5.1. Limitations

Both presented studies had a number of limitations. Our first study had a single-center design, which makes it non-generalizable for the general population. The patient history charts lacked data such as CVD risk factors, height, weight, or BMI. The TOF MRI images we used in this study visualize the blood flow in the posterior intracranial circulation rather than assess the anatomical properties of the vessels. BA diameter was calculated using BA area. The length of the VA V4 section was not measured, as there is no specific anatomical landmark, where the V3 section ends on a 3D vascular model. We could not include blood flow measurements in the different arteries as TCD examination was not part of the protocol to assess clinical patients. Therefore, we could not simulate blood flow in our models to estimate WSS in the vertebrobasilar system. WMH burden was assessed based on only FLAIR MRI sequence, which may produce artifacts in the infratentorial regions. Furthermore, lack of automated quantitative measurements for WMH area size limited the severity assessment. During our statistical analysis we used Mann-Whitney u test which only works as a method of selection. Significant results should be tested further to prove causal connection between the grouping variable and the examined variable. However, considering the number of variables measured, this was out of the scope of this paper.

In our second study our twin population is not an accurate representation of the general population. Neither of our studies contained flow velocity measurements of the vertebral arteries, there was no proof of weakened compensation of the non-dominant VA. Our monozygotic twin population was also significantly younger than our dizygotic and thus the exposure to environmental factors may have been shorter in this group. Lastly, although VA diameter difference showed higher monozygotic within-pair correlation, it did not fit the saturated model significantly. Consequently, no exact conclusion can be drawn from this finding except that the heritability of this parameter cannot be ruled out, and a larger population size is required to better understand this index.

6. CONCLUSIONS

In conclusion, we created a standardized and semi-automated technique to recreate and to measure the morphology of the vertebrobasilar system. Our data suggests that the severity of WMH burden is mainly influenced by age and hypertension, while the localization of the WMHs (or laterality) is mainly influenced by vessel morphology. In the VA region WMH burden was significantly higher on the non-dominant VA side. In the BA region WMH burden was significantly higher on the opposite side of the BA curve. Increased BA curvature with increased infratentorial lateral WMH burden may be a signal for inadequate blood flow and chronic ischemia. Our data showed that BA morphology may only effect PCA region WMHs when the posterior cerebral communicating arteries are hypoplastic or occluded. Further studies are needed to better understand the supratentorial effects of the BA morphology. VA dominance and the bending direction of the BA showed and opposite directional relationship meaning that a left dominant VA may lead to a right-side bending BA over decades. The length and volume of the BA showed moderate genetical influence. However, most of the measured morphological indices were influenced by shared and unshared environmental factors, which may highlight the complex hemodynamic background of the vertebrobasilar system. These findings support further collaborative initiatives to localize the specific genes involved in the vertebrobasilar system's development and regulation.

The potential clinical relevance of these findings is that it might play a role in the development of detecting intracranial hemodynamic disturbances and it may be used in future stroke prevention methods. However, further studies are needed to elucidate the associations between vertebrobasilar morphology and WMH severity.

7. SUMMARY

The vertebrobasilar system is unique in anatomical terms, as it is the only instance in the human body where a third artery is formed by the merging of two arteries. Asymmetrical vertebral artery (VA) flow and diameter are common findings, and the vertebral system is often left dominant. Unequal VA flow may lead to complex secondary blood flow patterns in the basilar artery (BA), which may cause bending of the artery over time. Increased VA diameter difference, tortuosity and torsion and increased BA curvature and tortuosity may cause oscillating and low wall shear stress, which plays an important role in the pathogenesis of atherosclerosis. These changes over time may lead to vertebrobasilar insufficiency. Increased white matter hyperintensity (WHM) burden has been considered as an indicator for inadequate blood perfusion on T2 weighted Fluid-attenuated inversion recovery images. The presence of WMH triples the risk of stroke and doubles the risk of dementia. Previous publications showed significant correlation between vertebrobasilar artery morphology and stroke localization. However, the connection between WMHs and large cerebral artery morphology is not yet fully understood. Furthermore, the genetic and environmental determinants influencing the development of the vertebrobasilar morphological indices are not yet clear.

We created a standardized and semi-automated technique to recreate and to measure the morphology of the vertebrobasilar system. We demonstrated that VA dominance influences the morphological indices of the BA. These changes correlate with WMH localization and burden. Increased bending direction of the BA with increased infratentorial lateral WMH burden may be a signal for inadequate blood flow in conjunction with chronic ischemia. We used the classical twin model and revealed that most of the VA and BA morphologic were influenced by shared and unshared factors which highlights the complex hemodynamical background of the vertebrobasilar system. BA length and volume showed moderate genetic influence.

8. ÖSSZEFOGLALÁS

A vertebrobasiláris rendszer anatómiai szempontból egyedülálló, mivel ez az egyetlen érrendszer az emberi testben, ahol két artéria összeömléséből egy új artéria keletkezik. Asszimetrikus arteria vertebralis (VA) áramlás és átmérő gyakran figyelhető meg rutin radiológiai vizsgálatok során , mely az esetek többségében bal domináns. Az egyenlőtlen VA áramlás következtében komplex másodlagos véráramlási mintázatok keletkeznek az arteria basilarisban (BA), melyek idővel az ér görbületének fokozódásához vezethet. Megnövekedett VA átmérő különbség, tortuozitás és torzió, valamint a megnövekedett BA görbület és tortuozitás alacsony és oszcilláló fali csúsztató-feszültséget okozhat, mely fontos szerepet játszik az érelmeszesedés patogenezisében. Ezek a változások idővel vertebrobasiláris inszufficienciához vezethetnek. Fokozott fehérállományi hiperintenzitás (WMH) terhelés az elégtelen perfúzió egyik indikátorának tekinthető T2 súlyozott Fluid-attenuated inversion recovery szekvencián. A WMH-k jelenléte megháromszorozza a stroke kockázatát és megduplázza a demencia kockázatát. A korábbi publikációk szignifikáns összefüggést mutattak a vertebrobasiláris rendszer morfológiája és a stroke lokalizációja között. Ugyanakkor a WMH-k és a vertebrobasiláris morfológia közötti kapcsolatot eddig még nem kutatták. Emellett a vertebrobasilári morfológiai indexek kialakulását befolyásoló genetikai és környezeti meghatározók még nem tisztázottak.

Kutatócsopurtunk egy standardizált vizsgálati protokollt hozott létre, mely alapján a vertebrobasiláris erek 3D rekonstrukcióját és fél-automata mérését végeztük. Kimutattuk, hogy a VA dominanciája befolyásolja a BA morfológiai tulajdonságait. Ezek a változások korrelálnak a WMH-k lokalizációjával és kiterjedésével. A BA görbületének és az infratentorialis WMH kiterjedésének növekedése az elégtelen perfúzió egyik előjele lehet. A klasszikus ikermodell segítségével kimutattuk, hogy a VA és a BA morfológiai változásainak többségét környezeti tényezők befolyásolták. A BA hossza és térfogata mérsékelt öröklődést mutatott.

9. BIBLIOGRAPHY

1. Haines, D.E., Chapter 8 - A Survey of the Cerebrovascular System, in Fundamental Neuroscience for Basic and Clinical Applications (Fifth Edition), D.E. Haines and G.A. Mihailoff, Editors., Elsevier, Philadelphia PA, 2018: p. 122-137.e121.

2. Mihailoff, G.A. and D.E. Haines, Chapter 12 - The Pons and Cerebellum, in Fundamental Neuroscience for Basic and Clinical Applications (Fifth Edition), D.E. Haines and G.A. Mihailoff, Editors., Elsevier, Philadelphia PA, 2018: p. 172-182.

3. Haines, D.E. and G.A. Mihailoff, Chapter 10 - An Overview of the Brainstem, in Fundamental Neuroscience for Basic and Clinical Applications (Fifth Edition), D.E. Haines and G.A. Mihailoff, Editors., Elsevier, Philadelphia PA, 2018: p. 152-159.

4. Bhadkaria, V., H. Chawre, S. JoshiS,D. JoshiS (2016) Histological variations in various segments of vertebral artery. Journal of Evolution of medical and Dental Sciences, 5: 120-126

5. London, G.M. (1997) Large arteries haemodynamics: conduit versus cushioning function. Blood Press Suppl, 2: 48-51

6. Wagner, H.P. and J.D. Humphrey (2011) Differential Passive and Active Biaxial Mechanical Behaviors of Muscular and Elastic Arteries: Basilar Versus Common Carotid. Journal of Biomechanical Engineering, 133

7. "morphology," Merriam-Webster.com Dictionary, URL: https://www.merriam-webster.com/dictionary/morphology. Accessed 10/3/2021.

8. Ghaffari, M., A. Alaraj, X. Du, X.J. Zhou, F.T. Charbel,A.A. Linninger (2018) Quantification of near-wall hemodynamic risk factors in large-scale cerebral arterial trees. Int J Numer Method Biomed Eng, 34: e2987

9. Wang, X., E. Liu, Z. Wu, F. Zhai, Y.C. Zhu, W. Shui,M. Zhou (2016) Skeleton-based cerebrovascular quantitative analysis. BMC Med Imaging, 16: 68

10. Wake-Buck, A.K., J.C. Gatenby,J.C. Gore (2012) Hemodynamic characteristics of the vertebrobasilar system analyzed using MRI-based models. PLoS One, 7: e51346

11. Zheng, J., B. Sun, R. Lin, Y. Teng, X. Zhao,Y. Xue (2021) Association between the vertebrobasilar artery geometry and basilar artery plaques determined by high-resolution magnetic resonance imaging. BMC Neurosci, 22: 20

12. Ravensbergen, J., J.K.B. Krijger, B. Hillen,H.W. Hoogstraten (1996) The influence of the angle of confluence on the flow in a vertebro-basilar junction model. Journal of Biomechanics, 29: 281-299

13. Ravensbergen, J., J.W. Ravensbergen, J.K. Krijger, B. Hillen,H.W. Hoogstraten (1998) Localizing role of hemodynamics in atherosclerosis in several human vertebrobasilar junction geometries. Arterioscler Thromb Vasc Biol, 18: 708-716

14. Fernandes, D.C., T.L.S. Araujo, F.R.M. Laurindo,L.Y. Tanaka, Chapter 7 - Hemodynamic Forces in the Endothelium: From Mechanotransduction to Implications on Development of Atherosclerosis, in Endothelium and Cardiovascular Diseases, P.L. Da Luz, et al., Editors., Academic Press, London, 2018: p. 85-95.

15. Nigro, P., J.-I. Abe,B.C. Berk (2011) Flow shear stress and atherosclerosis: a matter of site specificity. Antioxidants & redox signaling, 15: 1405-1414

16. Hwang, J., M.H. Ing, A. Salazar, B. Lassegue, K. Griendling, M. Navab, A. Sevanian,T.K. Hsiai (2003) Pulsatile versus oscillatory shear stress regulates NADPH oxidase subunit expression: implication for native LDL oxidation. Circ Res, 93: 1225-1232

17. Sho, E., M. Sho, T.M. Singh, C. Xu, C.K. Zarins,H. Masuda (2001) Blood flow decrease induces apoptosis of endothelial cells in previously dilated arteries resulting from chronic high blood flow. Arterioscler Thromb Vasc Biol, 21: 1139-1145

18. Choy, M., V. Ganesan, D.L. Thomas, J.S. Thornton, E. Proctor, M.D. King, L. van der Weerd, D.G. Gadian,M.F. Lythgoe (2006) The chronic vascular and haemodynamic response after permanent bilateral common carotid occlusion in newborn and adult rats. J Cereb Blood Flow Metab, 26: 1066-1075

19. Sho, E., H. Nanjo, M. Sho, M. Kobayashi, M. Komatsu, K. Kawamura, C. Xu, C.K. Zarins,H. Masuda (2004) Arterial enlargement, tortuosity, and intimal thickening in response to sequential exposure to high and low wall shear stress. J Vasc Surg, 39: 601-612

20. Sho, E., M. Komatsu, M. Sho, H. Nanjo, T.M. Singh, C. Xu, H. Masuda,C.K. Zarins (2003) High flow drives vascular endothelial cell proliferation during

flow-induced arterial remodeling associated with the expression of vascular endothelial growth factor. Exp Mol Pathol, 75: 1-11

21.   Sho, M., E. Sho, T.M. Singh, M. Komatsu, A. Sugita, C. Xu, H. Nanjo, C.K. Zarins,H. Masuda (2002) Subnormal shear stress-induced intimal thickening requires medial smooth muscle cell proliferation and migration. Exp Mol Pathol, 72: 150-160

22.   Hiroki, M., K. Miyashita,M. Oda (2002) Tortuosity of the white matter medullary arterioles is related to the severity of hypertension. Cerebrovasc Dis, 13: 242-250

23.   Poni, E.S., B.H. Liwnicz, Y. Ying-Ying,M. North (2003) Tortuosity of terminal arterioles in the basal ganglia is increased in status lacunaris. Invest Clin, 44: 137-145

24.   Han, H.C. (2012) Twisted blood vessels: symptoms, etiology and biomechanical mechanisms. J Vasc Res, 49: 185-197

25.   Ballermann, B.J., A. Dardik, E. Eng,A. Liu (1998) Shear stress and the endothelium. Kidney Int Suppl, 67: S100-108

26.   Burke, G.M., A.M. Burke, A.K. Sherma, M.C. Hurley, H.H. Batjer,B.R. Bendok (2009) Moyamoya disease: a summary. Neurosurg Focus, 26: E11

27.   Zhou, L., Y. Yan, H. Du, X. Ni, G. Wang,Q. Wang (2020) Plaque features and vascular geometry in basilar artery atherosclerosis. Medicine (Baltimore), 99: e19742

28.   Lee, S.H., N. Hur,S.K. Jeong (2012) Geometric analysis and blood flow simulation of basilar artery. J Atheroscler Thromb, 19: 397-401

29.   Yu, J., S. Zhang, M.L. Li, Y. Ma, Y.R. Dong, M. Lou, F. Feng, S. Gao, S.W. Wu,W.H. Xu (2018) Relationship between the geometry patterns of vertebrobasilar artery and atherosclerosis. BMC Neurol, 18: 83

30.   Chen, Z., A.F. Liu, H. Chen, C. Yuan, L. He, Y. Zhu, M. Guan, W.J. Jiang,X. Zhao (2016) Evaluation of basilar artery atherosclerotic plaque distribution by 3D MR vessel wall imaging. J Magn Reson Imaging, 44: 1592-1599

31.   Deng, S., J. Zheng, Y. Wu, D. Yang, H. Chen, B. Sun, Y. Xue,X. Zhao (2021) Geometrical characteristics associated with atherosclerotic disease in the basilar artery: a magnetic resonance vessel wall imaging study. Quant Imaging Med Surg, 11: 2711-2720

32. Libby, P., J.E. Buring, L. Badimon, G.K. Hansson, J. Deanfield, M.S. Bittencourt, L. Tokgozoglu,E.F. Lewis (2019) Atherosclerosis. Nat Rev Dis Primers, 5: 56

33. Lima Neto, A.C., R. Bittar, G.S. Gattas, E. Bor-Seng-Shu, M.L. Oliveira, R.D.C. Monsanto,L.F. Bittar (2017) Pathophysiology and Diagnosis of Vertebrobasilar Insufficiency: A Review of the Literature. Int Arch Otorhinolaryngol, 21: 302-307

34. Chuang, Y.M., C.Y. Liu, P.J. Pan,C.P. Lin (2008) Posterior communicating artery hypoplasia as a risk factor for acute ischemic stroke in the absence of carotid artery occlusion. J Clin Neurosci, 15: 1376-1381

35. Savitz, S.I. and L.R. Caplan (2005) Vertebrobasilar disease. N Engl J Med, 352: 2618-2626

36. Posterior Circulation Ischemia: Specific Vascular Sites and Conditions, in Vertebrobasilar Ischemia and Hemorrhage: Clinical Findings, Diagnosis and Management of Posterior Circulation Disease, L.R. Caplan, Editor., Cambridge University Press, Cambridge, 2015: p. 179-213.

37. Sati, P., I.C. George, C.D. Shea, M.I. Gaitan,D.S. Reich (2012) FLAIR*: a combined MR contrast technique for visualizing white matter lesions and parenchymal veins. Radiology, 265: 926-932

38. de Leeuw, F.E., J.C. de Groot, E. Achten, M. Oudkerk, L.M. Ramos, R. Heijboer, A. Hofman, J. Jolles, J. van Gijn,M.M. Breteler (2001) Prevalence of cerebral white matter lesions in elderly people: a population based magnetic resonance imaging study. The Rotterdam Scan Study. J Neurol Neurosurg Psychiatry, 70: 9-14

39. Moroni, F., E. Ammirati, M.A. Rocca, M. Filippi, M. Magnoni,P.G. Camici (2018) Cardiovascular disease and brain health: Focus on white matter hyperintensities. Int J Cardiol Heart Vasc, 19: 63-69

40. Kim, K.W., J.R. MacFall,M.E. Payne (2008) Classification of white matter lesions on magnetic resonance imaging in elderly persons. Biol Psychiatry, 64: 273-280

41. Wardlaw, J.M., M.C. Valdes Hernandez,S. Munoz-Maniega (2015) What are white matter hyperintensities made of? Relevance to vascular cognitive impairment. J Am Heart Assoc, 4: 001140

42. Debette, S. and H.S. Markus (2010) The clinical importance of white matter

hyperintensities on brain magnetic resonance imaging: systematic review and meta-analysis. BMJ, 341: c3666

43. DeCarli, C., E. Fletcher, V. Ramey, D. Harvey,W.J. Jagust (2005) Anatomical mapping of white matter hyperintensities (WMH): exploring the relationships between periventricular WMH, deep WMH, and total WMH burden. Stroke, 36: 50-55

44. Griffanti, L., M. Jenkinson, S. Suri, E. Zsoldos, A. Mahmood, N. Filippini, C.E. Sexton, A. Topiwala, C. Allan, M. Kivimaki, A. Singh-Manoux, K.P. Ebmeier, C.E. Mackay,G. Zamboni (2018) Classification and characterization of periventricular and deep white matter hyperintensities on MRI: A study in older adults. Neuroimage, 170: 174-181

45. Wahlund, L.O., F. Barkhof, F. Fazekas, L. Bronge, M. Augustin, M. Sjogren, A. Wallin, H. Ader, D. Leys, L. Pantoni, F. Pasquier, T. Erkinjuntti, P. Scheltens,C. European Task Force on Age-Related White Matter (2001) A new rating scale for age-related white matter changes applicable to MRI and CT. Stroke, 32: 1318-1322

46. Topcuoglu, M.A. (2012) Transcranial Doppler ultrasound in neurovascular diseases: diagnostic and therapeutic aspects. J Neurochem, 123 Suppl 2: 39-51

47. Society for Vascular Ultrasound. (SVU) (2019). Intracranial Cerebrovascular Evaluation Transcranial Doppler (Non-Imaging) and Transcranial Duplex Imaging (TCDI). Retrieved 2021.09.24 from: https://higherlogicdownload.s3. amazonaws.com/SVUNET/c9a8d83b-2044-4a4e-b3ec-cd4b2f542939/ UploadedImages/PPG_Docs/2__Intracranial_Cerebrovascular_Evaluation_ Transcranial_Doppler__Non-Imaging__and_Transcranial_Duplex_Imaging__ TCDI___Updated_2019_.pdf.

48. Babikian, V.L., E. Feldmann, L.R. Wechsler, D.W. Newell, C.R. Gomez, U. Bogdahn, L.R. Caplan, M.P. Spencer, C. Tegeler, E.B. Ringelstein,A.V. Alexandrov (2000) Transcranial Doppler ultrasonography: year 2000 update. J Neuroimaging, 10: 101-115

49. Dittrich, R. and E.B. Ringelstein (2008) Occurrence and clinical impact of microembolic signals during or after cardiosurgical procedures. Stroke, 39: 503-511

50. Arkuszewski, M., M. Swiat, R.W. Hurst, J.B. Weigele, R.N. Al-Okaili, S.E. Kasner, E.R. Melhem,J. Krejza (2012) Vertebral and Basilar Arteries: Transcranial Color-Coded Duplex Ultrasonography versus Conventional TCD in Detection of Narrowings. Neuroradiol J, 25: 509-514

51. Schulte-Altedorneburg, G., D.W. Droste, V. Popa, W.A. Wohlgemuth, M. Kellermann, D.G. Nabavi, L. Csiba,E.B. Ringelstein (2000) Visualization of the basilar artery by transcranial color-coded duplex sonography : comparison with postmortem results. Stroke, 31: 1123-1127

52. Yang, J., Y. Hua, X. Li, M. Gao, Q. Li, B. Liu,L. Jiao (2018) The Assessment of Diagnostic Accuracy for Basilar Artery Stenosis by Transcranial Color-Coded Sonography. Ultrasound Med Biol, 44: 995-1002

53. Vymazal, J., A.M. Rulseh, J. Keller,L. Janouskova (2012) Comparison of CT and MR imaging in ischemic stroke. Insights Imaging, 3: 619-627

54. Kishore, L.T. and P.C. Gupta (2013) Vascular imaging:Past, present & future. Journal International Medical Sciences Academy, 26: 65-68

55. Schuknecht, B. (2004) Latest techniques in head and neck CT angiography. Neuroradiology, 46: s208-s213

56. Khan, S., P. Rich, A. Clifton,H.S. Markus (2009) Noninvasive detection of vertebral artery stenosis: a comparison of contrast-enhanced MR angiography, CT angiography, and ultrasound. Stroke, 40: 3499-3503

57. Mattle, H.P., M. Arnold, P.J. Lindsberg, W.J. Schonewille,G. Schroth (2011) Basilar artery occlusion. Lancet Neurol, 10: 1002-1014

58. Goldmakher, G.V., E.C. Camargo, K.L. Furie, A.B. Singhal, L. Roccatagliata, E.F. Halpern, M.J. Chou, T. Biagini, W.S. Smith, G.J. Harris, W.P. Dillon, R.G. Gonzalez, W.J. Koroshetz,M.H. Lev (2009) Hyperdense basilar artery sign on unenhanced CT predicts thrombus and outcome in acute posterior circulation stroke. Stroke, 40: 134-139

59. Sohn, Y.H., H.Y. Cheon, P. Jeon,S.Y. Kang (2004) Clinical implication of cerebral artery calcification on brain CT. Cerebrovasc Dis, 18: 332-337

60. Caplan, L. (2000) Posterior circulation ischemia: then, now, and tomorrow. The Thomas Willis Lecture-2000. Stroke, 31: 2011-2023

61. Shishikura, D. (2016) Noninvasive imaging modalities to visualize atherosclerotic plaques. Cardiovasc Diagn Ther, 6: 340-353

62. Ryu, C.W., H.S. Kwak, G.H. Jahng,H.N. Lee (2014) High-resolution MRI of intracranial atherosclerotic disease. Neurointervention, 9: 9-20

63. Xiao, Y.D., R. Paudel, J. Liu, C. Ma, Z.S. Zhang,S.K. Zhou (2016) MRI contrast agents: Classification and application (Review). Int J Mol Med, 38: 1319-1326

64. Hartung, M.P., T.M. Grist,C.J. Francois (2011) Magnetic resonance angiography: current status and future directions. J Cardiovasc Magn Reson, 13: 19

65. Miyazaki, M. and V.S. Lee (2008) Nonenhanced MR angiography. Radiology, 248: 20-43

66. Hong, J.M., C.S. Chung, O.Y. Bang, S.W. Yong, I.S. Joo,K. Huh (2009) Vertebral artery dominance contributes to basilar artery curvature and peri-vertebrobasilar junctional infarcts. J Neurol Neurosurg Psychiatry, 80: 1087-1092

67. Ngo, M.T., H.S. Kwak,G.H. Chung (2020) Change in basilar artery length and bending according to aging and vertebral artery dominance: A longitudinal study. Sci Rep, 10: 8904

68. Jeong, S.K., J.H. Lee, D.H. Nam, J.T. Kim, Y.S. Ha, S.Y. Oh, S.H. Park, S.H. Lee, N. Hur, H.S. Kwak,G.H. Chung (2015) Basilar artery angulation in association with aging and pontine lacunar infarction: a multicenter observational study. J Atheroscler Thromb, 22: 509-517

69. Zhu, W., Y.F. Wang, X.F. Dong, H.X. Feng, H.Q. Zhao,C.F. Liu (2016) Study on the correlation of vertebral artery dominance, basilar artery curvature and posterior circulation infarction. Acta Neurol Belg, 116: 287-293

70. Nishikata, M., Y. Hirashima, T. Tomita, R. Futatsuya, Y. Horie,S. Endo (2004) Measurement of basilar artery bending and elongation by magnetic resonance cerebral angiography: relationship to age, sex and vertebral artery dominance. Arch Gerontol Geriatr, 38: 251-259

71. Nigro, P., J. Abe,B.C. Berk (2011) Flow shear stress and atherosclerosis: a matter of site specificity. Antioxid Redox Signal, 15: 1405-1414

72. Xu, Z., M. Li, J. Lyu, Z. Hou, J. He, D. Mo, F. Gao, X. Liu, B. Sui, M. Shen, Y. Pan, Y. Wang, X. Lou, Z. Miao, B. Luo,N. Ma (2020) Different risk factors in identical features of intracranial atherosclerosis plaques in the posterior and anterior circulation in high-resolution MRI. Ther Adv Neurol Disord, 13: 1756286420909991

73. Zhang, D.P., S.L. Zhang, J.W. Zhang, H.T. Zhang, S.Q. Fu, M. Yu, Y.F. Ren,P. Ji (2014) Basilar artery bending length, vascular risk factors, and pontine infarction. J Neurol Sci, 338: 142-147

74. Kim, B.J. and J.S. Kim (2014) Ischemic stroke subtype classification: an asian

viewpoint. J Stroke, 16: 8-17

75. Tarnoki, A.D., B. Fejer, D.L. Tarnoki, L. Littvay, P. Lucatelli, C. Cirelli, F. Fanelli, B. Sacconi, C. Fagnani, E. Medda, F. Farina, G. Meneghetti, T. Horvath, G. Pucci, G. Schillaci, M.A. Stazi,C. Baracchini (2017) Vertebral Artery Diameter and Flow: Nature or Nurture. J Neuroimaging, 27: 499-504

76. Stewart, C.R., M.S. Stringer, Y. Shi, M.J. Thrippleton,J.M. Wardlaw (2021) Associations Between White Matter Hyperintensity Burden, Cerebral Blood Flow and Transit Time in Small Vessel Disease: An Updated Meta-Analysis. Front Neurol, 12: 647848

77. Marstrand, J.R., E. Garde, E. Rostrup, P. Ring, S. Rosenbaum, E.L. Mortensen,H.B. Larsson (2002) Cerebral perfusion and cerebrovascular reactivity are reduced in white matter hyperintensities. Stroke, 33: 972-976

78. Chen, Y., X. Wang, L. Guan,Y. Wang (2021) Role of White Matter Hyperintensities and Related Risk Factors in Vascular Cognitive Impairment: A Review. Biomolecules, 11

79. Rosenberg, G.A., A. Wallin, J.M. Wardlaw, H.S. Markus, J. Montaner, L. Wolfson, C. Iadecola, B.V. Zlokovic, A. Joutel, M. Dichgans, M. Duering, R. Schmidt, A.D. Korczyn, L.T. Grinberg, H.C. Chui,V. Hachinski (2016) Consensus statement for diagnosis of subcortical small vessel disease. J Cereb Blood Flow Metab, 36: 6-25

80. Nagy, M., M.U. Azeem, Y. Soliman, S.A. Nawab, A.H. Jun-O'Connell, R.P. Goddeau, Jr., M. Moonis, B. Silver,N. Henninger (2019) Pre-existing White Matter Hyperintensity Lesion Burden and Diagnostic Certainty of Transient Ischemic Attack. J Stroke Cerebrovasc Dis, 28: 944-953

81. Fu, J.H., C.Z. Lu, Z. Hong, Q. Dong, Y. Luo,K.S. Wong (2005) Extent of white matter lesions is related to acute subcortical infarcts and predicts further stroke risk in patients with first ever ischaemic stroke. J Neurol Neurosurg Psychiatry, 76: 793-796

82. Zerna, C., A.Y.X. Yu, J. Modi, S.K. Patel, J.I. Coulter, E.E. Smith,S.B. Coutts (2018) Association of White Matter Hyperintensities With Short-Term Outcomes in Patients With Minor Cerebrovascular Events. Stroke, 49: 919-923

83. Jeerakathil, T., P.A. Wolf, A. Beiser, J. Massaro, S. Seshadri, R.B. D'Agostino,C. DeCarli (2004) Stroke risk profile predicts white matter hyperintensity volume: the Framingham Study. Stroke, 35: 1857-1861

84. Ten Kate, M., C.H. Sudre, A. den Braber, E. Konijnenberg, M.G. Nivard, M.J. Cardoso, P. Scheltens, S. Ourselin, D.I. Boomsma, F. Barkhof,P.J. Visser (2018) White matter hyperintensities and vascular risk factors in monozygotic twins. Neurobiol Aging, 66: 40-48

85. Sachdev, P.S., A. Thalamuthu, K.A. Mather, D. Ames, M.J. Wright, W. Wen,O.C.R. Team (2016) White Matter Hyperintensities Are Under Strong Genetic Influence. Stroke, 47: 1422-1428

86. Sahu, M. and J.G. Prasuna (2016) Twin Studies: A Unique Epidemiological Tool. Indian J Community Med, 41: 177-182

87. Maes, H.H., ACE Model, in Encyclopedia of Statistics in Behavioral Science, B.S. Everitt and D.C. Howell, Editors., John Wiley & Sons, Inc., Chichester, 2005: p. 5-10.

88. Tatu, L., T. Moulin, F. Vuillier,J. Bogousslavsky (2012) Arterial territories of the human brain. Front Neurol Neurosci, 30: 99-110

89. Pari, A. (2014) Main characteristics of Hungarian twin and multiple births in official statistics. Twin Res Hum Genet, 17: 359-368

90. Heath, A.C., D.R. Nyholt, R. Neuman, P.A. Madden, K.K. Bucholz, R.D. Todd, E.C. Nelson, G.W. Montgomery,N.G. Martin (2003) Zygosity diagnosis in the absence of genotypic data: an approach using latent class analysis. Twin Res, 6: 22-26

91. Thierfelder, K.M., A.B. Baumann, W.H. Sommer, M. Armbruster, C. Opherk, H. Janssen, M.F. Reiser, A. Straube,L. von Baumgarten (2014) Vertebral artery hypoplasia: frequency and effect on cerebellar blood flow characteristics. Stroke, 45: 1363-1368

92. Del Brutto, O.H., R.M. Mera, V.J. Del Brutto, A.F. Costa, M. Zambrano,J. Brorson (2017) Basilar Artery Dolichoectasia: Prevalence and Correlates With Markers of Cerebral Small Vessel Disease in Community-Dwelling Older Adults. J Stroke Cerebrovasc Dis, 26: 2909-2914

93. Roth, W., S. Morgello, J. Goldman, J.P. Mohr, M.S. Elkind, R.S. Marshall,J. Gutierrez (2017) Histopathological Differences Between the Anterior and Posterior Brain Arteries as a Function of Aging. Stroke, 48: 638-644

94. Del Brutto, V.J., J.G. Ortiz,J. Biller (2017) Intracranial Arterial Dolichoectasia. Front Neurol, 8: 344

95. Vieco, P.T., E.E. Maurin, 3rd,C.E. Gross (1997) Vertebrobasilar dolichoectasia:

evaluation with CT angiography. AJNR Am J Neuroradiol, 18: 1385-1388

96.   Strassburger, T.L., H.C. Lee, E.M. Daly, J. Szczepanik, J.S. Krasuski, M.J. Mentis, J.A. Salerno, C. DeCarli, M.B. Schapiro,G.E. Alexander (1997) Interactive effects of age and hypertension on volumes of brain structures. Stroke, 28: 1410-1417

97.   Klimek-Piotrowska, W., M. Kopec, M. Kochana, R.M. Krzyzewski, K.A. Tomaszewski, P. Brzegowy,J. Walocha (2013) Configurations of the circle of Willis: a computed tomography angiography based study on a Polish population. Folia Morphol (Warsz), 72: 293-299

98.   Katsanos, A.H., M. Kosmidou, A.P. Kyritsis,S. Giannopoulos (2013) Is vertebral artery hypoplasia a predisposing factor for posterior circulation cerebral ischemic events? A comprehensive review. Eur Neurol, 70: 78-83

99.   Caplan, L.R. (2007) Arterial occlusions: does size matter? J Neurol Neurosurg Psychiatry, 78: 916

100.   Yuan, S.M. (2016) Aberrant Origin of Vertebral Artery and its Clinical Implications. Braz J Cardiovasc Surg, 31: 52-59

101.   Kwon, H.M., J.H. Kim, J.S. Lim, J.H. Park, S.H. Lee,Y.S. Lee (2009) Basilar artery dolichoectasia is associated with paramedian pontine infarction. Cerebrovasc Dis, 27: 114-118

102.   Zhao, B., J.G. Ibrahim, Y. Li, T. Li, Y. Wang, Y. Shan, Z. Zhu, F. Zhou, J. Zhang, C. Huang, H. Liao, L. Yang, P.M. Thompson,H. Zhu (2019) Heritability of Regional Brain Volumes in Large-Scale Neuroimaging and Genetic Studies. Cereb Cortex, 29: 2904-2914

10. BIBLIOGRAPHY OF THE CANDIDATE'S PUBLICATIONS

10.1. Publications related to the present thesis

1. **Szalonai, L.**, Jokkel, Zs., Horvath, T., Forgo, B., Kalina, I., Maurovich-Horvat, P., Auyang, P.L., Zubair, M.M., Garami, Zs., Tarnoki, D.L., Tarnoki, A.D. (2021). Laterality of deep white matter hyperintensities correlates with basilar artery bending and vertebral artery dominance. Croatian Medical Journal, 62 : 4 pp. 360-366. , 7 p.
   IF: 1.351

2. **Szalontai, L.**, Jokkel, Zs., Horvath, T., Piroska, M., Forgo, B., Olah, Cs., Kostyal, L., Tarnoki, D.L., Tarnoki, A.D. (2021). Are the Morphological Indices of the Vertebrobasilar System Heritable? A Twin Study Based on 3D Reconstructed Models. Medicina-Lithuania, 57 : 2 Paper: 127 , 10 p.
   IF: 2.430

Articles in Hungarian

1. **Szalontai, L**,. Tárnoki, A.D., Tarnoki, D.L., Garami, Zs. (2018). Transcranialis Dopplervizsgálati protokoll: a Houston Methodist Hospital gyakorlata és a magyar metodika összevetése. Magyar Radiológia Online, 9 : 2 pp. 4/1-9. , 9 p.

10.2. Publications not related to the present thesis

1. Hernyes, A., Piroska, M., Fejer, B., **Szalontai, L.**, Szabo, H., Forgo, B., Jermendy, A.L., Molnar, A.A., Maurovich-Horvat, P., Jermendy, Gy., Merkely, B., Tarnoki D.L., Tarnoki A.D. (2021). Overlapping Genetic Background of Coronary Artery and Carotid/Femoral Atherosclerotic Calcification. Medicina-Lithuania, 57 : 3 Paper: 252 , 18 p.   IF: 2.430

2. Tarnoki, A.D., **Szalontai, L.,*** ; Fagnani, C.,* ; Tarnoki, D.L., Lucatelli, P., Maurovich-Horvat, P., Jermendy, A.L., Kovacs, A., Molnar, A.A., Godor, E., Fejer, B., Hernyes, A., Cirelli, C., Fanelli, F., Farina, F., Baracchini, C., Meneghetti, G., Gyarmathy, A.V., Jermendy, Gy., Merkely, B., Pucci, G., Schillaci, G., Stazi, M.A., Medda, E. (2021). Genetic and environmental factors on heart rate, mean arterial pressure and carotid intima media thickness: a longitudinal twin study. Cardiology Journal, 28 : 3 pp. 431-438. , 8 p.
IF: 2.737

3. Forgo, B., Medda, E., Hernyes, A,. **Szalontai, L,.** Tarnoki, D.L., Tarnoki, A.D. (2018). Carotid Artery Atherosclerosis: A Review on Heritability and Genetics. Twin Research And Human Genetics, 21 : 5 pp. 333-346. , 14 p.
IF: 1.159

4. Forgo, B., Tarnoki, A.D., Tarnoki, D.L., Kovacs, D.T., **Szalontai, L.**, Persely, A., Hernyes, A., Szily, M., Littvay, L., Medda, E., Szabo, A., Kozak, L.R., Rudas, G., Sas, A., Sepsi, M., Kostyal, L., Olah, Cs. (2018). Are the Variants of the Circle of Willis Determined by Genetic or Environmental Factors? Results of a Twin Study and Review of the Literature. Twin Research And Human Genetics, 21 : 5 pp. 384-393. , 10 p.
IF: 1.159

Articles in Hungarian

1. Hernyes, A., Fejér, B., Szabó, H., **Szalontai, L**., Persely, A., Fekete, M., Szily, M., Jokkel, Z., Debreceni, R., Gyulai, K., Szabo, G., Zoldi, L., Tarnoki, A.D., Tarnoki D.L. (2019). Az arteria carotis communis intima-media komplex sajátosságainak vizsgálata ultrahanggal - Technikai megfontolások és korrelációk egyéb atherosclerosisra utaló változókkal. Magyar Radiológia Online, 10 : 3 pp. 1-10. , 10 p.

2. Szavcsur, P., Horváth, B., **Szalontai, L**., Csemez, I., Bártfai, R., Schneider, F., Strausz, T., Gődény, M. (2019). Percutan, ultrahangvezérelt FNAB a nyelőcső nyaki szakaszán elhelyezkedő carcinoma igazolására. Magyar Radiológia Online, 10 : 4 pp. 5/1-4. , 4 p.

3. Santirso, D., Kovács, D., **Szalontai, L**., Diaz, O., Lumsden, A., Garami, Zs. (2018). Nyitva vagy zárva: ez a nagy kérdés! Magyar Radiológia Online, 9 : 1 pp. 6/1-5. , 5 p.

4. **Szalontai, L**., Tárnoki, A.D., Tárnoki, D.L., Garami, Zs. (2018). Carotis-ultrahangvizsgálati protokoll: a houstoni és a magyar metodika összevetése. Magyar Radiológia Online, 9 : 3 pp. 2/1-14. , 14 p.

Cumulative impact factor of the candidate's publications related to the thesis: **3.781**

Cumulative impact factor of the candidate's publications not related to the

thesis: 7.485

Total cumulative impact factor of the candidate's publications: 11.266

11. ACKNOWLEDGMENTS

First, I would like to thank my loving and beautiful wife Éva, for planting the seed of thought in my head to pursue a PhD five years ago. She patiently listened to all my theories and was my rehearsal audience for all my presentations.

I would like to express my sincerest gratitude to my mentors Adam and David Tarnoki for taking me under their wings as a PhD candidate. It was my privilege that I could join their research team in the Medical Imaging Centre of Semmelweis University. The years of guidance and encouragement along the right scientific path has helped me grow into my potential. They taught me how to stand my own ground and always believed in me. I would not be where I am today without them.

I would like to thank my parents who supported and accompanied me on this five-year endeavor.

And last, I would like to thank all my former co-authors who I shared ideas, concepts and plans to further science together. I would like to thank Zsolt Garami, Tamás Horváth, Bianka Forgó, Márton Piroska, Csaba Oláh, Laszló Kostyál, Viktor Bérczi and Pál Maurovich-Horvát for their continuous support and contribution to my research. I have been fortunate to be surrounded by such a great and talented team.

11.1. Funding